Research Square

Preprints are preliminary reports that have not undergone peer review.
They should not be considered conclusive, used to inform clinical practice,
or referenced by the media as validated information.

Sodium selenite mitigates hyperglycemia-aggravated cerebral ischemia/reperfusion injury via the p53/PUMA apoptotic pathway

Lan Yang
Ningxia Medical University
Tianxiang Zheng
Ningxia Medical University
Xida Yin
Ningxia Medical University
Feng Ding
Ningxia Medical University
Shuai Zhao
Ningxia Hui Autonomous Region People's Hospital
Yajuan Fu
Ningxia Medical University
Yue Chang
Ningxia Medical University
Zhiyao Lian
Chongqing Medical University
Xinyan Zhao
Third Affiliated Hospital of Zhengzhou University
Li Jing
19970015@nxmu.edu.cn

Ningxia Medical University

Research Article

Keywords: Cerebral ischemia/reperfusion injury, Hyperglycemia, Sodium selenite, Selenoprotein H, p53/puma pathway

Posted Date: April 10th, 2026

DOI: https://doi.org/10.21203/rs.3.rs-9183531/v1

License: This work is licensed under a Creative Commons Attribution 4.0 International License.
Read Full License

Additional Declarations: No competing interests reported.

Abstract

Hyperglycemia aggravates cerebral ischemia/reperfusion (I/R) injury, a severe ischemic stroke complication with few treatments. Selenium exerts neuroprotective effects, yet its molecular mechanisms in this injury remain unclear. This study explored whether sodium selenite alleviates the injury via regulating the p53/PUMA apoptotic pathway and the role of selenoprotein H (SelH). In vivo, Sprague-Dawley rats (including PUMA-knockdown models) were subjected to middle cerebral artery occlusion/reperfusion; in vitro, HT22 cells (PUMA-knockdown/SelH-overexpressing) were treated with high glucose and oxygen-glucose deprivation/reoxygenation. Results showed hyperglycemia exacerbated neurological deficits, infarct volume, neuronal apoptosis and mitochondrial damage in vivo, and induced ROS overproduction, mitochondrial dysfunction and apoptosis in vitro. Sodium selenite reversed these injuries, downregulated p53/PUMA pathway-related proteins, upregulated the bcl-2/Bax ratio, and elevated SelH expression. PUMA knockdown enhanced its neuroprotection, while SelH overexpression attenuated cell damage by inhibiting the p53/PUMA pathway (not direct oxidative stress reduction). Thus, sodium selenite mitigates hyperglycemia-aggravated cerebral I/R injury through the SelH-p53/PUMA pathway, providing novel therapeutic targets for diabetic stroke.

1. Introduction

Ischemic stroke has become one of the greatest threats to human health [1]. Thrombolysis to restore blood perfusion in the ischemic area is currently the most effective intervention, but it is limited by a narrow time window (≤4.5 hours), leaving only a small proportion of patients benefiting [2]. Moreover, reperfusion itself can induce secondary cerebral ischemia/reperfusion (I/R) injury [3]. Diabetes/hyperglycemia, as an independent risk factor for stroke, increases the incidence of stroke by 1.8-6.0 folds [4]. During cerebral I/R, neurons, glial cells (astrocytes, microglia), and endothelial cells produce large amounts of ROS [5-7], disrupting antioxidant homeostasis and triggering lipid peroxidation and macromolecular damage [8-9]. The hyperglycemic environment synergistically activates multiple cell death pathways including apoptosis, necrosis, ferroptosis, and autophagy, leading to neuronal death [10-12]. Therefore, exploring the mechanisms by which hyperglycemia aggravates cerebral I/R injury is of great significance for developing preventive and therapeutic strategies for hyperglycemia-exacerbated cerebral I/R injury.

Apoptosis plays a crucial role in promoting the progression of cerebral I/R injury. Cell apoptosis is tightly regulated by the p53 (tp53, tp63, tp73) family. p63 can mediate puma expression to regulate endoplasmic reticulum stress-induced apoptosis [13], while p73 mediates oxidative stress by modulating the Bax/bcl-2 ratio. Downstream members of the bcl-2 family (Bax/Bak) in the p53 pathway play key roles in apoptosis, promoting cell death by inducing changes in mitochondrial outer membrane permeability and caspase cascade reactions [14-16]. This pathway has been validated in intervention models, where inhibiting puma expression alleviates apoptosis-related damage [17]. Our previous work has demonstrated that hyperglycemia significantly exacerbates cerebral I/R injury by upregulating mitochondrial apoptotic factors, including cleaved caspase-3, cleaved caspase-9, and cytochrome c [18].

However, the specific molecular mechanisms underlying the involvement of the p53/PUMA apoptotic pathway in hyperglycemia-aggravated cerebral ischemic injury remain largely elusive, which provides a direction for subsequent research.

Selenium (Se) is an essential trace element in humans with antioxidant properties [19]. Selenium exerts its biological effects mainly through selenoproteins. Selenoprotein P, glutathione peroxidase 4 (GPX4), and selenoprotein W are the three most abundantly expressed selenoproteins in the brain, playing core roles in brain function and participating in various physiological activities such as regulating energy metabolism, nutrient uptake, and ion balance in neural cells [20]. Previous studies have found that Se can significantly increase the expression level of selenoprotein H (SelH). Downregulation of SelH is closely associated with the process of neuronal oxidative damage in diseases such as Alzheimer's disease and Parkinson's disease [21]. Our previous work demonstrated that selenium alleviates cerebral I/R injury under hyperglycemic conditions by regulating mitochondrial dynamics and optimizing mitochondrial function [22]. However, whether selenium exerts protective effects through other molecular mechanisms remains unclear. Meanwhile, the mechanism of SelH in cerebrovascular diseases, especially its regulatory role in the apoptotic pathway under hyperglycemic I/R pathological conditions, lacks systematic research.

In summary, hyperglycemia significantly exacerbates cerebral I/R injury through multiple pathways including oxidative stress and apoptosis, while the regulatory mechanisms of apoptosis in the hyperglycemic environment await further clarification. Based on the well-established effects of selenium in antagonizing oxidative damage and inhibiting apoptosis [22-26], and the central role of the p53/puma pathway in mediating neural cell death in cerebral I/R injury [27-29], this study aims to systematically reveal the molecular mechanism by which selenium alleviates hyperglycemia-synergized cerebral I/R neural injury through targeted regulation of the p53/puma apoptotic signaling pathway, providing a novel target for the treatment of diabetes mellitus complicated with stroke.

2. Materials and methods

2.1. Animals and grouping

This study was approved by the Animal Ethics Committee of Ningxia Medical University (Approval Number: IACUC-NYLAC-2023-038). Specific pathogen-free (SPF) male Sprague-Dawley rats were housed in a pathogen-free environment (humidity 55% ± 5%, 12 h light/12 h dark cycle, room temperature 22℃ ± 2℃) with free access to water and food. The experiment included 7 groups (n=10/group): Sham operation (Sham), normoglycemic MCAO 30 min/reperfusion 24 h (NG+I/R 24 h), normoglycemic MCAO 30 min/reperfusion 72 h (NG+I/R 72 h), hyperglycemic MCAO 30 min/reperfusion 24 h (HG+I/R 24 h), hyperglycemic MCAO 30 min/reperfusion 72 h (HG+I/R 72 h), hyperglycemic + Sodium selenite + MCAO 30 min/reperfusion 24 h (HG+Se+I/R 24 h), and hyperglycemic + Sodium selenite + MCAO 30 min/reperfusion 72 h (HG+Se+I/R 72 h). puma gene-knockdown SD rats (Shanghai Model Organisms

Center, Inc., Approval Number: IACUC-NNYLAC-2023-206) were divided into NG+I/R 24 h, HG+I/R 24 h, and HG+Se+I/R 24 h groups.

2.2. Animal model establishment and treatment

The hyperglycemia model and MCAO model were established as described in our previous study [22]. Rats were fasted for 24 h with free access to water before the experiment, and baseline body weight was measured. Streptozotocin (STZ) solution (1%, 60 mg/kg) was injected intraperitoneally into the left lower abdomen. After injection, animals were housed in an IVC independent ventilation cage system, with standard feed and 5% glucose solution provided ad libitum. 72 h after administration, fasting blood glucose concentration was detected via tail vein blood sampling. Rats meeting the diabetic model criteria (fasting blood glucose ≥16.7 mmol/L persistently) were randomly assigned to the diabetic model group and the selenium intervention group.

After successful establishment of the hyperglycemia model, Sodium selenite (#214485, SIGMA-ALDRICH, USA) was dissolved in normal saline to prepare a 0.04 mg/mL injection, which was administered intraperitoneally to hyperglycemic rats at a concentration of 0.4 mg/kg/d for 4 consecutive weeks.

The middle cerebral artery occlusion (MCAO)/reperfusion model was established using the suture method. After weighing, experimental animals were anesthetized with isoflurane inhalation anesthesia system (oxygen flow rate 1.5 L/min, induction concentration 3%). During the anesthesia maintenance period (maintenance concentration 1.5%), animals were fixed in the supine position on the operating table. A polylysine suture (diameter 0.26 mm) was advanced intracranially through the external carotid artery incision until slight resistance was encountered. The suture was removed after 30 min of occlusion to restore blood flow, establishing reperfusion models at 24 h and 72 h time points. For the Sham group, all surgical procedures were performed except for vascular occlusion. After surgery, all animals were placed in a constant temperature monitoring system (37 ± 0.5℃) until awakening.

2.3. 2,3,5-triphenyltetrazolium chloride (TTC) staining and neurological deficit evaluation

Cerebral infarct volume was quantified by TTC staining. Serial coronal sections (thickness 2 mm) were prepared with a pre-cooled microtome and placed in 12-well cell culture plates. Sections were completely immersed in 2% TTC solution (pH 7.4). Infarcted areas appeared pale white, while normal brain tissue appeared bright red. Images of whole brain sections were captured, and infarct volume was scanned and calculated using ImageJ software.

Neurological function of MCAO model rats was quantitatively evaluated using the Bederson scoring system. Standardized behavioral tests were performed 24 h after 30 min of occlusion followed by reperfusion, with a score ≥1 as the criterion for successful model establishment. Scoring criteria: 0 points, no neurological deficit; 1 point, flexion and adduction of the contralateral forelimb when

suspended by the tail; 2 points, combined with decreased resistance in the contralateral push test; 3 points, spontaneous circling towards the ischemic side on the basis of the above.

2.4. Hematoxylin-eosin (HE) staining and Nissl staining

Brain tissues fixed with 4% paraformaldehyde and embedded in paraffin were cut into 4 μm serial coronal sections. After baking, sections were deparaffinized with xylene and gradient ethanol sequentially. For HE staining (G1129, Solarbio, China), sections were dehydrated and cleared, then mounted with neutral balsam. Whole sections were scanned to count the proportion of pyknotic neurons for evaluating cell apoptosis. For Nissl staining, another batch of sections was deparaffinized similarly, incubated with Nissl staining solution (G1430, Servicebio, China), rinsed gently, dehydrated with gradient ethanol, cleared with xylene, and mounted with neutral balsam. Nissl-positive cells were observed and counted under a fluorescence microscope, and mean optical density was measured to quantify Nissl body abundance, reflecting neuronal protein synthesis activity and damage degree.

2.5. Transmission electron microscopy

Immediately after reperfusion, the brain was removed by decapitation on ice, and 1 mm^3 brain slices from the junction of the right infarct focus were collected. Samples were fixed with 2.5% glutaraldehyde at 4℃ overnight, rinsed with phosphate buffer, and post-fixed with 1% osmium tetroxide. After gradient dehydration with acetone, transition with propylene oxide, infiltration and polymerization with Epon-812 resin, the embedded blocks were trimmed. Sections were double-stained with uranyl acetate and lead citrate, rinsed with deionized water, and dried. Mitochondria, nuclear membrane, and cytoplasmic structures were observed using an HT7800 electron microscope at 80 kV, and images were captured randomly.

2.6. Cell culture and drug treatment

Mouse hippocampal neuronal HT22 cell line (Hysigen, China, Cat.#TCM-C821), puma-knockdown HT22 stable cell line (sipuma-HT22, Species: Mouse; GeneBank: NM_133234), and SelH-overexpressing HT22 stable cell line (SelH-HT22, Species: Mouse; GeneBank: NM_001033166) were purchased from Guangzhou Jingrui Biotechnology Co., Ltd. HT22 cells were cultured in DMEM/F12 medium (#C3130-0500, VivaCell, China) supplemented with 10% fetal bovine serum (A5669701, Thermo Fisher, China) and 1% penicillin/streptomycin (#03-031-5B, Biological Industries, Israel) in an incubator at 37℃ with 5% CO_2. A concentration of 50 mmol/L was used as the high glucose medium to treat cells. Healthy HT22 cells were seeded into culture flasks or 6-well plates under optimal growth conditions. After cell adhesion, the medium was replaced with HG medium for 24 h to establish a high glucose environment. A concentration of 100 nmol/L was used as the high selenium medium to pretreat HT22 cells for 24 h.

2.7. Oxygen-glucose deprivation/reoxygenation (OGD/R) model and experimental cell grouping

An in vitro model was established to simulate the pathological process of I/R. According to experimental design requirements, the culture medium was replaced with glucose-free DMEM medium, and cells were

transferred to a tri-gas incubator (1% O_2, 5% CO_2, 94% N_2) for 4 h of continuous hypoxia exposure. After terminating hypoxia intervention, the initial culture system corresponding to each experimental group was restored, and cells were cultured under normoxic conditions for another 24 h to establish the in vitro reperfusion injury model.

puma-knockdown HT22 stable cells were divided into four groups: Vector group (cultured in high selenium and normal glucose medium for 24 h, followed by OGD for 4 h and reoxygenation for 24 h); NG+Se group (cultured in high selenium and normal glucose medium for 24 h, followed by OGD for 4 h and reoxygenation for 24 h); HG+Se group (sipuma-HT22 cells cultured in high glucose and high selenium medium for 24 h, followed by OGD/R); HG+Se+Ipatasertib group (cultured in high glucose and high selenium medium supplemented with puma activator Ipatasertib for 24 h, followed by OGD for 4 h and reoxygenation for 24 h).

SelH-HT22 cells were divided into five groups: Control group (cultured in normal glucose medium for 24 h, followed by OGD/R); HG group (cultured in high glucose medium for 24 h, followed by OGD for 4 h and reoxygenation for 24 h); HG+Ipatasertib group (cultured in high glucose medium supplemented with Ipatasertib for 24 h, followed by OGD for 4 h and reoxygenation for 24 h); HG+CLZ-8 group (cultured in high glucose medium supplemented with puma inhibitor CLZ-8 for 24 h, followed by OGD for 4 h and reoxygenation for 24 h); HG+CLZ-8+Ipatasertib group (cultured in high glucose medium supplemented with both CLZ-8 and Ipatasertib for 24 h, followed by OGD for 4 h and reoxygenation for 24 h).

2.8. CCK-8 assay for cell viability

Cells were seeded into 96-well plates and cultured normally until adhesion. According to the experimental grouping, each group had 6 replicate wells. After corresponding treatments, 10 μL of CCK-8 solution (CK04, DOJINDO, Japan) was added to each well, followed by incubation at 37℃ in the dark for 2 h. The absorbance (OD value) was measured using a microplate reader.

2.9. Tunel staining

After completing cell climbing and paraffin section interventions according to grouping, paraffin sections were treated with proteinase K for 20 min, and cell climbing slices were fixed with 4% paraformaldehyde for 10 min. Permeabilization was performed with 0.5% Triton X-100 for 5 min. Each slice was added with 200 μL Equilibration Buffer and incubated at room temperature for 30 min. After discarding the buffer, 50 μL TdT incubation buffer was added, and incubation was carried out at 37℃ in the dark for 1 h. Hoechst 33342 was added to counterstain cell nuclei, and images were observed under a microscope.

2.10. Western blot

Cerebral ischemic penumbra tissues or cells were lysed with RIPA buffer, homogenized, and centrifuged at 12,000 r/min at 4℃ to collect the supernatant. Protein concentration was determined by BCA assay. Samples were denatured at 95℃, separated by 8-12% SDS-PAGE, and transferred to PVDF membranes (Millipore, USA) at 400 mA for 23 min. Membranes were blocked with 5% non-fat milk for 1 h, then

incubated overnight with primary antibodies against puma (1:500, #24633, CST, USA), bcl-2 (1:1000, Rabbit, #sc-7382, Santa, USA), p-p53 (1:1000, #2526, CST, USA), p53 (1:1000, #2524, CST, USA), cleaved caspase-3 (1:1000, Rabbit, #9661, CST, USA), caspase-3 (1:1000, #9662, CST, USA), cleaved caspase-9 (1:500, #9509, CST, USA), Bax (1:1000, Rabbit, #41162, CST, USA), and β-actin (1:5000, #bs-0061R, Biosynthesis, China). Membranes were then incubated with goat anti-mouse IgG (H+L) secondary antibody (1:50000, #abs20040, Absin, China) or goat anti-rabbit IgG (H+L) secondary antibody (1:50000, #S0002, Affinity, USA) at room temperature for 2 h. ECL development was performed, and bands were analyzed using ImageJ software.

2.11. Immunofluorescence staining

After preparing cell climbing slices and completing interventions according to grouping, cells were fixed with 4% paraformaldehyde for 10 min and permeabilized with 0.5% Triton X-100 for 5 min. Blocking was performed with goat serum at 37℃ for 30 min. Primary antibodies against puma (1:200), p53 (1:200), bcl-2 (1:200), and bax (1:500) were added and incubated at 4℃ overnight. Corresponding species-specific fluorescent secondary antibodies (goat anti-rabbit or goat anti-mouse, 1:1000) were added and incubated at 37℃ in the dark for 2 h. Hoechst 33342 was added to counterstain nuclei, and images were captured using a confocal microscope (Olympus).

2.12. DHE fluorescent probe

5 mg of DHE was dissolved in 1.58 mL of DMSO to prepare a 10 mmol/L stock solution, which was stored at -20℃ in the dark. After completing interventions on cell climbing slices in 24-well plates, 1 mL of medium and 10 μL of DHE stock solution were added to each well, followed by incubation at 37℃ for 30 min. Climbing slices were taken out and inverted on glass slides, and images were captured using a slice fluorescence scanner.

2.13. Mitochondrial membrane potential

Working solution was prepared by adding 5 μL JC-1 (200×) to 1 mL buffer. 1 mL of medium and 1 mL of JC-1 working solution were added to each well of a 24-well plate, followed by incubation at 37℃ for 20 min. Slices were washed twice with JC-1 buffer, counterstained with Hoechst 33342, inverted on glass slides, and observed under a fluorescence microscope for image capture.

2.14. Statistical analysis

Experimental data were analyzed using SPSS Statistics 27.0, and visualization was performed using GraphPad Prism 10. Quantitative data were expressed as mean ± standard deviation. Independent samples t-test was used for comparisons between two groups; one-way analysis of variance (ANOVA) was used for comparisons among multiple groups, and LSD post-hoc test was performed for pairwise comparisons if significant differences existed among groups. The significance level was set at $\alpha = 0.05$, and $P < 0.05$ was considered statistically significant.

3. Results

3.1. Sodium selenite alleviates infarct volume and neurological dysfunction in hyperglycemia-aggravated cerebral I/R injury in vivo

In vivo evaluations of infarct volume and neurological dysfunction were performed in rats of each group. Morphological results (Fig. 1A) and body weight changes (Fig. 1B) showed that the diabetic model group exhibited typical diabetic signs such as withered yellow fur and nutritional metabolic disorders after STZ induction, with progressive weight loss, in contrast to the gradual weight gain in the NG group. Although Sodium selenite intervention did not significantly reverse weight loss, fur condition and activity were improved compared with the model group. Final body weights were 322.9 ± 10.25 g in the NG group, 236.0 ± 2.646 g in the HG group ($P < 0.05$), and 244.0 ± 8.718 g in the HG+Se group ($P < 0.05$). Blood glucose levels were detected subsequently (Fig. 1C). After successful model establishment, blood glucose was significantly elevated in the diabetic model groups (29.17 ± 1.710 mmol/L in the HG group and 26.87 ± 3.758 mmol/L in the HG+Se group), showing significant differences compared with the NG group (7.033 ± 0.3215 mmol/L, $P < 0.05$). Although Sodium selenite intervention did not significantly improve glucose metabolism, all model groups maintained persistent hyperglycemia (>16.7 mmol/L), meeting experimental requirements. TTC staining was used to evaluate changes in cerebral infarct area (Fig. 1D and 1E). The NG+I/R group showed well-demarcated pale white infarcts, while the HG+I/R group had a significantly larger infarct area compared with the NG+I/R group ($P < 0.05$). In contrast, the HG+Se+I/R group showed a significant reduction in infarct area compared with the HG+I/R group ($P < 0.05$).

Neurological behavioral scoring using the Berderson scale (Fig. 1F) showed that compared with the Sham group (0 points, no neurological abnormalities), the HG+I/R model group had a significantly higher neurological function score than the NG+I/R model group ($P < 0.05$), indicating that hyperglycemia exacerbates neurological damage after cerebral ischemia. Notably, the hyperglycemic model group supplemented with Sodium selenite had a significantly lower neurological function score than the untreated hyperglycemic model group ($P < 0.05$).

Transmission electron microscopy results (Fig. 1G) further showed that neurons in the Sham group had intact structures, regular nuclear morphology, elliptical mitochondria with clear cristae. After 24 h of I/R, the NG+I/R 24h group exhibited damage characteristics such as nuclear shrinkage, chromatin dissolution, mitochondrial swelling, and decreased cristae. In the NG+I/R 72h group, nuclear pyknosis was alleviated, and some mitochondrial morphology was restored. The HG+I/R 24h group showed the most severe damage, including significant nuclear pyknosis, mitochondrial vacuolization, and loss of cristae, with no significant improvement at 72 h. In the HG+Se+I/R group, intact nuclear morphology and well-preserved mitochondrial structures with clear cristae were observed at both 24 h and 72 h time points.

Tunel assay was used to evaluate brain tissue apoptosis (Fig. 1H). Only a small number of apoptotic cells were observed in the Sham group. After 24 h of I/R (Fig. 1I), cell apoptosis increased significantly

(P < 0.05), and the proportion of apoptotic cells further increased in the HG+I/R 24h group (P < 0.05), while the number of apoptotic neurons was significantly reduced in the HG+Se+I/R 24h group compared with the HG+I/R 24h group (P < 0.05). After 72 h of I/R (Fig. 1J), brain tissue apoptosis increased, and the HG+I/R 72h group had more apoptotic cells than the NG+I/R 72h group (P < 0.05), while the HG+Se+I/R 72h group had significantly fewer apoptotic neurons than the HG+I/R 72h group (P < 0.05). These results suggest that Sodium selenite can effectively inhibit neuronal ultrastructural damage and cell apoptosis induced by hyperglycemia-aggravated cerebral I/R.

3.2. Sodium selenite attenuates tissue edema and neuronal apoptosis in hyperglycemia-aggravated cerebral I/R injury in vivo

HE staining and Nissl staining were used for systematic pathological evaluation of neurons in the penumbral cortex and deep medulla of both ischemic and non-ischemic brain tissues. Fig. 2A shows neuronal damage in the penumbral cortex and deep medulla of the ischemic side. HE staining results (Fig. 2C and 2G) showed that neurons in the Sham group had uniformly stained cytoplasm and intact nuclear membranes. After 24 h of I/R, the NG+I/R group exhibited changes such as pale cytoplasm, loose extracellular matrix, and condensed nuclear chromatin (P < 0.05). The HG+I/R group showed further aggravated damage, characterized by irreversible changes including wrinkled neuronal nuclear membranes and extensive nuclear fragmentation and dissolution (P < 0.05). In the HG+Se+I/R group, cerebral edema was alleviated, and the number of pyknotic neurons was significantly reduced compared with the HG+I/R group (P < 0.05). After 72 h of cerebral I/R, the change trends in each group were similar to those at 24 h after I/R (P < 0.05), but the degree of brain tissue damage in each group was recovered compared with 24 h after I/R (Fig. 2D and 2H).

Neuronal functional status was evaluated by Nissl staining. These basophilic granules are mainly enriched in rough endoplasmic reticulum-ribosome complexes, and changes in their density can reflect neuronal metabolic activity. In the Sham group, deeply stained Nissl granules were uniformly distributed in cortical and medullary neurons, indicating that cells maintained normal protein synthesis function. After 24 h of I/R (Fig. 2E and 2I), the proportion of neurons containing Nissl bodies was significantly reduced in the NG+I/R group (P < 0.05). Pathological damage was exacerbated in the HG+I/R model group, with a further decrease in the proportion of neurons containing Nissl bodies (P < 0.05), confirming that hyperglycemia can synergistically aggravate post-ischemic neuronal dysfunction. In the HG+Se+I/R group, the proportion of neurons containing Nissl bodies was higher than that in the HG+I/R group, and cell function was improved (P < 0.05). After 72 h of cerebral I/R, Nissl bodies in the penumbral cortex and medulla of each group were significantly recovered compared with 24 h (Fig. 2F and 2J).

Stroke not only directly damages the ischemic brain tissue but may also indirectly affect the non-ischemic brain tissue through neural plasticity and inflammatory responses. Fig. 2B shows neuronal damage in the penumbral cortex and deep medulla of the non-ischemic side. HE staining results (Fig. 2K, 2L, 2O, and 2P) showed that in the cerebral cortex and medulla after 24h and 72h of I/R, the NG+I/R group had pale-stained brain tissue and a small number of pyknotic cells (P < 0.05). The HG+I/R group

had more neurons with nuclear pyknosis and mild edema ($P < 0.05$). In the HG+Se+I/R group, cerebral edema was alleviated, and the number of pyknotic cells was reduced compared with the HG+I/R group ($P < 0.05$). Nissl staining results (Fig. 2M, 2N, 2Q, and 2R) showed that in the non-ischemic side of rat brain tissue, after 24h and 72h of I/R, cells in the NG+I/R group were vacuolated, and Nissl bodies were slightly reduced ($P < 0.05$). In the HG+I/R group, the number of Nissl bodies in brain tissue was significantly less than that in the NG+I/R group ($P < 0.05$). In the HG+Se+I/R group, Nissl bodies were more abundant than those in the HG+I/R group, and cell function was improved ($P < 0.05$). In summary, Sodium selenite can improve the morphology and function of neurons on both ischemic and non-ischemic sides 24h and 72h after I/R, help maintain cell status, and thereby alleviate hyperglycemia-aggravated cerebral I/R injury.

3.3. Sodium selenite regulates the p53/puma apoptotic signaling pathway to inhibit hyperglycemia-aggravated cerebral I/R injury in vivo

GO function enrichment and KEGG pathway enrichment analyses were performed on differentially expressed proteins. KEGG pathways were mainly enriched in p53 signaling pathway, cytoplasmic DNA sensing pathway, extrinsic apoptotic signaling pathway, autophagosome assembly, type 2 diabetes mellitus pathway, insulin resistance pathway, Alzheimer's disease pathway, axon guidance pathway, and gonadotropin-releasing hormone signaling pathway (Fig. 3A). GO functional terms were mainly involved in oxidative stress, cellular response to DNA damage, regulation of tyrosine kinase signaling, mitochondrial calcium import, positive regulation of locomotion, response to inorganic substances, and regulation of cell population proliferation (Fig. 3B). In this study, immunofluorescence (Fig. 3C, 3D) and Western blot (Fig. 3K) were used to systematically observe changes in the expression of apoptotic factors such as p53/puma and bcl-2/Bax in the cerebral ischemic penumbra of rats after I/R. At 24 h after cerebral I/R (Fig. 3E, 3G, and 3I), the relative fluorescence intensities of puma and p53 in neurons were significantly higher in the NG+I/R 24h and HG+I/R 24h groups than in the Sham group ($P < 0.05$), while the fluorescence intensity ratio of bcl-2/Bax was significantly lower ($P < 0.05$). In the HG+Se+I/R 24h group, the relative fluorescence intensities of puma and p53 were significantly decreased ($P < 0.05$), and the fluorescence intensity ratio of bcl-2/Bax was significantly increased ($P < 0.05$). At 72 h after I/R, the fluorescence intensities of puma, p53, and bcl-2/Bax showed similar trends to those at 24h after cerebral I/R (Fig. 3F, 3H, 3J). Western blot results further verified the above findings (Fig. 3L, 3M, 3N, 3O, and 3P): compared with the Sham group, the expressions of puma, p-p53/p53, cleaved caspase-9, and cleaved caspase-3/caspase-3 were significantly increased ($P < 0.05$), and the bcl-2/Bax ratio was significantly decreased ($P < 0.05$) in all I/R groups. Compared with the NG+I/R 24h group, the expressions of puma, p-p53/p53, cleaved caspase-9, and cleaved caspase-3/caspase-3 were significantly increased ($P < 0.05$), and the bcl-2/Bax ratio was significantly decreased ($P < 0.05$) in the HG+I/R 24h group. After Sodium selenite intervention, compared with the HG+I/R 24h group, the expressions of puma, p-p53/p53, cleaved caspase-9, and cleaved caspase-3/caspase-3 were significantly decreased ($P < 0.05$), and the bcl-2/Bax ratio was significantly increased ($P < 0.05$) in the HG+Se+I/R 24h group. At the 72h I/R time point, compared with the HG+I/R 72h group, the expressions of puma and p-p53/p53 were still significantly decreased ($P < 0.05$), and the bcl-2/Bax ratio was

significantly increased ($P < 0.05$) in the HG+Se+I/R 72h group, while the expressions of cleaved caspase-3/caspase-3 and cleaved caspase-9 showed no significant changes. These results indicate that hyperglycemia can exacerbate changes in the expression of apoptosis-related proteins after I/R injury, while Sodium selenite exerts long-term neuroprotective effects by continuously inhibiting the p53/puma pathway and restoring the balance of bcl-2/Bax, thereby significantly reducing neuronal apoptosis.

3.4. Sodium selenite attenuates high glucose-OGD/R-induced HT22 cell damage in vitro

The protective effect of Sodium selenite pretreatment against OGD/R-induced neuronal damage was evaluated (Fig. 4A, 4B). Compared with the Control group, cell viability was significantly decreased in all intervention groups ($P < 0.05$). Under normal glucose conditions, cell viability was significantly higher in the NG+Se+OGD/R group than in the NG+OGD/R group ($P < 0.05$). The high glucose environment exacerbated OGD/R damage, as evidenced by a further decrease in cell viability in the HG+OGD/R group compared with the NG+OGD/R group ($P < 0.05$). Cell viability was significantly improved in the Sodium selenite intervention group compared with the HG+OGD/R group ($P < 0.05$).

Semi-quantitative analysis of neuronal ROS levels using DHE probe (Fig. 4A, 4C) showed that after OGD/R treatment, ROS levels were significantly increased in all groups ($P < 0.05$). ROS levels were significantly higher in the HG+OGD/R group than in the NG+OGD/R group ($P < 0.05$). ROS levels were significantly lower in the NG+OGD/R+Se group than in the NG+OGD/R group ($P < 0.05$), and significantly lower in the HG+OGD/R+Se group than in the HG+OGD/R group ($P < 0.05$). These results indicate that high glucose can enhance ROS production in OGD/R neurons, while Sodium selenite intervention can inhibit ROS production in high glucose-OGD/R neuronal cells.

JC-10 staining was used to detect mitochondrial membrane potential levels (Fig. 4D, 4E). After OGD/R treatment, mitochondrial membrane potential levels were significantly decreased in all groups compared with the Control group ($P < 0.05$). Mitochondrial membrane potential levels were significantly lower in the HG+OGD/R group than in the NG+OGD/R group ($P < 0.05$). After Sodium selenite intervention, mitochondrial membrane potential levels were significantly increased in the NG+OGD/R+Se group ($P < 0.05$), and significantly higher in the HG+OGD/R+Se group than in the HG+OGD/R group ($P < 0.05$).

Meanwhile, Tunel kit was used for cell apoptosis staining to detect cell apoptosis levels (Fig. 4F, 4G). There were few apoptotic cells in the Control group. After OGD/R treatment, the apoptotic rate of cells in each group showed a significant upward trend ($P < 0.05$). The number of apoptotic cells was significantly increased in the NG+OGD/R and HG+OGD/R groups compared with the Control group ($P < 0.05$), significantly lower in the NG+OGD/R+Se group than in the NG+OGD/R group ($P < 0.05$), and significantly fewer in the HG+OGD/R+Se group than in the HG+OGD/R group ($P < 0.05$). These results suggest that high glucose can increase ROS production, decrease mitochondrial membrane potential, and promote cell apoptosis, while Sodium selenite can reduce apoptosis of high glucose-OGD/R neurons.

3.5. Sodium selenite reduces high glucose-OGD/R-induced HT22 cell damage by inhibiting the p53/puma apoptotic pathway in vitro

Immunofluorescence labeling of p53, puma, bcl-2, and Bax was used to observe the relative fluorescence intensities of high glucose-OGD/R HT22 cells. Immunofluorescence results of p53 and puma (Fig. 5A, 5B, and 5C) and bcl-2 and Bax (Fig. 5D, 5E) showed that neurons in the Control group exhibited uniform spatial distribution, good cell morphology, low staining levels of p53 and puma, and a relatively high bcl-2/Bax ratio. After OGD/R, the relative fluorescence intensities of p53 and puma were significantly increased ($P < 0.05$), and the bcl-2/Bax ratio was decreased ($P < 0.05$) in the NG+OGD/R and HG+OGD/R groups. Compared with the NG+OGD/R group, the relative fluorescence intensities of p53 and puma were significantly decreased ($P < 0.05$), and the bcl-2/Bax ratio was significantly increased ($P < 0.05$) in the NG+OGD/R+Se group. Compared with the HG+OGD/R group, the relative fluorescence intensities of p53 and puma were significantly decreased ($P < 0.05$), and the bcl-2/Bax ratio was significantly increased ($P < 0.05$) in the HG+OGD/R+Se group.

Western blot was also used to detect changes in apoptosis-related proteins such as puma, p-p53/p53, cleaved caspase-9, cleaved caspase-3/caspase-3, and bcl-2/Bax in each group (Fig. 5F). As shown in Fig. 5H, 5I, 5J, and 5K, the expressions of puma, p-p53/p53, cleaved caspase-9, and cleaved caspase-3/caspase-3 were low in the Control group. After OGD/R, the expressions of puma, p-p53/p53, cleaved caspase-9, and cleaved caspase-3/caspase-3 were increased to varying degrees ($P < 0.05$). Compared with the NG+OGD/R group, the expressions of puma, p-p53/p53, cleaved caspase-9, and cleaved caspase-3/caspase-3 were significantly increased ($P < 0.05$) in the HG+OGD/R group. Compared with the NG+OGD/R group, the NG+OGD/R+Se group showed decreased expressions of puma, p-p53/p53, cleaved caspase-9, and cleaved caspase-3/caspase-3 ($P < 0.05$); similarly, these expressions were decreased in the HG+OGD/R+Se group compared with the HG+OGD/R group ($P < 0.05$). Notably, the expression ratio of bcl-2/Bax showed an opposite trend to the above pro-apoptotic factors (Fig. 5G). The expression of bcl-2/Bax was higher in the Control group, but significantly decreased in all groups after OGD/R intervention ($P < 0.05$). Compared with the HG+OGD/R group, the expression of bcl-2/Bax was significantly increased in the HG+OGD/R+Se group ($P < 0.05$). These results indicate that high glucose can significantly enhance neuronal apoptosis in the OGD/R model. Sodium selenite pretreatment can inhibit the expressions of p53 and puma, specifically regulate the balance of bcl-2/Bax protein expression, and effectively reverse the apoptotic cascade induced by hyperglycemia-synergized I/R.

3.6. Puma downregulation attenuates high glucose-OGD/R-induced HT22 cell damage in vitro

To evaluate the effects of high glucose-OGD/R and puma knockdown on HT22 cells, puma-knockdown stable cell lines were used. Western blot was used to detect puma protein levels in cells (Fig. 6A, 6B) to verify puma downregulation. Cell status was observed under an inverted microscope, and CCK-8 assay was used to detect the viability of HT22 cells in each group after puma knockdown (Fig. 6C, 6G). In the Vector group, the number of cells was reduced, and some cell processes were shortened or disappeared. In the NG+Se group, cells were uniformly distributed, spindle-shaped, in relatively good condition, and

cell viability was significantly enhanced ($P < 0.05$). In the HG+Se group, the number of cells was significantly decreased, nuclear structures were blurred, the proportion of pyknotic cells was significantly increased, cell growth status was poor, and cell viability was significantly lower than that in the NG+Se group ($P < 0.05$). In the HG+Se+Ipatasertib group, cell damage was further aggravated, the number of cells was further reduced, and cell viability was further decreased ($P < 0.05$).

DHE probe was used to detect ROS levels in puma-knockdown HT22 cells after OGD/R in each group (Fig. 6D, 6H). Compared with the control group (Vector), the NG+Se group significantly inhibited ROS production ($P < 0.05$), while the HG+Se group significantly promoted ROS generation ($P < 0.05$). In addition, Ipatasertib intervention further exacerbated ROS accumulation ($P < 0.05$).

JC-1 was used to detect mitochondrial membrane potential (Fig.s 6E, 6I). Mitochondrial membrane potential was significantly increased in the NG+Se group ($P < 0.05$), inhibited in the HG+Se group ($P < 0.05$), and further decreased after Ipatasertib intervention ($P < 0.05$).

Tunel kit was used to detect cell apoptosis (Fig. 6F, 6J). There were more apoptotic cells in the Vector group. After puma knockdown, the number of apoptotic cells was significantly reduced in the NG+Se group ($P < 0.05$). The number of apoptotic cells in the HG+Se group after high glucose intervention was significantly higher than that in the NG+Se group ($P < 0.05$). After Ipatasertib intervention, the number of apoptotic cells in the HG+Se+Ipatasertib group was significantly higher than that in the HG+Se group ($P < 0.05$). These results suggest that high glucose-OGD/R leads to decreased cell viability, increased ROS production, decreased mitochondrial membrane potential, and cell apoptosis. puma deficiency reduces such damage, while the use of the activator Ipatasertib increases the damage caused by high glucose-OGD/R.

3.7. Puma downregulation reduces high glucose-OGD/R-induced HT22 cell damage by inhibiting the p53/puma apoptotic pathway in vitro

Immunofluorescence was used to observe the expressions of p53, puma (Fig. 7A, 7C, and 7D), and bcl-2/Bax (Fig. 7B, 7E) in puma-knockdown cells. In the Vector group, the expressions of p53 and puma were relatively obvious, and the bcl-2/Bax ratio was low. In the puma-knockdown NG+Se group, the expressions of p53 and puma were significantly decreased ($P < 0.05$), and the bcl-2/Bax ratio was significantly increased ($P < 0.05$). Compared with the NG+Se group, the expressions of p53 and puma were significantly increased ($P < 0.05$), and the bcl-2/Bax ratio was significantly decreased ($P < 0.05$) in the HG+Se group. After Ipatasertib intervention, the expressions of p53 and puma were further increased ($P < 0.05$), and the bcl-2/Bax ratio was further decreased ($P < 0.05$) in the HG+Se+Ipatasertib group.

Western blot was used to detect the protein expressions of puma, p-p53/p53, cleaved caspase-9, cleaved caspase-3/caspase-3, Bax, and bcl-2 (Fig. 7F). Quantitative results are shown in Fig. 7H, 7I, 7J, and 7K. In the Vector group, the expressions of puma, p-p53/p53, and cleaved caspase-9 were relatively high, while the expression of cleaved caspase-3/caspase-3 was low. In the NG+Se group, the expressions of puma, p-p53/p53, and cleaved caspase-9 were significantly decreased ($P < 0.05$).

Compared with the NG+Se group, the expressions of puma, p-p53/p53, cleaved caspase-3/caspase-3, and cleaved caspase-9 were significantly increased ($P < 0.05$) in the HG+Se group. The expressions of puma, p-p53/p53, cleaved caspase-3/caspase-3, and cleaved caspase-9 in the HG+Se+Ipatasertib group were significantly higher than those in the HG+Se group ($P < 0.05$). The expression level of bcl-2/Bax showed dynamic changes opposite to the above pro-apoptotic factors (Fig. 7G). Experimental results indicate that decreased puma can also reduce p53 expression, suggesting that p53 not only regulates puma expression but also puma may reversely affect p53 expression levels.

3.8. Critical role of puma downregulation in sodium selenite-alleviated hyperglycemic cerebral I/R injury in vivo

Puma gene-knockdown rats were used. HE staining showed (upper row of Fig. 8A) that neurons in NG+I/R group had basically intact structures with only mild pale cytoplasm. The HG+I/R group had increased numbers of neurons with nuclear pyknosis and cytoplasmic vacuolization. In the Sodium selenite intervention group, cell morphology was restored, and the number of pyknotic neurons was reduced. Nissl staining results (lower row of Fig. 8A) showed that in NG+I/R group, neurons were arranged neatly, cell bodies were plump, and Nissl bodies in the cytoplasm were abundant and uniformly distributed. In HG+I/R group, the degree of Nissl body loss was significantly increased. In the Sodium selenite intervention group, neuronal morphology was further restored, and the number of Nissl bodies in the cytoplasm was significantly increased.

Tunel assay showed (Fig. 8B) that there were very few apoptotic cells in the NG+I/R group, a slight increase in apoptotic positive cells in the HG+I/R group, and a decrease in the number of apoptotic positive cells in the HG+Se+I/R group. Fluorescence staining results (Fig. 8C, 8D) showed that the fluorescence intensities of p53 and puma were weak in the NG+I/R group, with strong bcl-2 signal and weak Bax signal, and a high bcl-2/Bax ratio. In the HG+I/R group, the fluorescence intensities of p53/puma were significantly enhanced, and the bcl-2/Bax ratio was significantly decreased. In the HG+Se+I/R group, the fluorescence intensities of p53/puma were decreased, and the bcl-2/Bax ratio was increased again.

Western blot was used to detect the protein expressions of puma, p-p53/p53, cleaved caspase-9, cleaved caspase-3/caspase-3, Bax, and bcl-2 (Fig. 8E). Fig. 8I shows that in the expression of p-p53/p53, the Vector group had the lowest expression, the HG+I/R group had a significant increase ($P < 0.05$), and the HG+Se+I/R group was significantly lower than the HG+I/R group ($P < 0.05$). Fig.s 8G, 8H, and 8J show that the expressions of puma, cleaved caspase-3/caspase-3, and cleaved caspase-9 were low in the NG+I/R group, significantly higher in the HG+I/R group than in the NG+I/R group ($P < 0.05$), and significantly lower in the HG+Se+I/R group than in the HG group ($P < 0.05$). The trend of bcl-2/Bax was opposite to the above apoptotic factors (Fig. 8F). The expression of bcl-2/Bax was low in the Vector group, significantly increased in the NG+I/R group ($P < 0.05$), significantly lower in the HG+I/R group than in the NG+I/R group ($P < 0.05$), and significantly lower in the HG+Se+I/R group than in the HG+I/R group ($P < 0.05$). These results indicate that puma downregulation can significantly reduce neuronal apoptosis

induced by hyperglycemic I/R. Sodium selenite amplifies the anti-apoptotic effect by downregulating p53, puma, cleaved caspase-9, and cleaved caspase-3 and upregulating the bcl-2/Bax ratio, thereby significantly reducing neuronal damage induced by hyperglycemic cerebral I/R.

3.9. SelH overexpression attenuates high glucose-OGD/R-induced HT22 cell damage by regulating puma in vitro

The antioxidant effect of sodium selenite is one of the key factors for its upregulation of SelH expression. Western blot was used to detect the expression of SelH (Fig. 9A, 9B). The expression level of SelH in the NG+Se group was significantly higher than that in the NG group. Therefore, SelH-overexpressing HT22 cells were constructed for experiments. The status of SelH-overexpressing HT22 cells was observed under an inverted microscope (Fig. 9C), and CCK-8 assay was used to detect the viability of SelH-overexpressing HT22 cells (Fig. 9D). The normal glucose OGD/R group (Control) had abundant cells in good condition. In the HG+OGD/R group, the number of cells was slightly reduced, the number of pyknotic cells was slightly increased, cell growth status was poor, and there was no significant difference in cell viability. In the HG+OGD/R+Ipatasertib activator group, cell damage was further aggravated, and the number of cells was further reduced ($P < 0.05$). In the HG+OGD/R+CLZ-8 inhibitor group, the number of cells was significantly increased, cell status was significantly improved, and morphology tended to be normal ($P < 0.05$). In HG+OGD/R+CLZ-8+Ipatasertib group, the number of cells was between that of the HG+Ipatasertib group and the HG+CLZ-8 group, morphology was good, and cell viability was decreased compared with the HG+CLZ-8 group ($P < 0.05$).

For ROS levels (Fig. 9E, 9F), ROS expression in the HG group was slightly higher than that in the Control group, and significantly higher in the HG+Ipatasertib group than in the HG group ($P < 0.05$). In contrast, ROS expression was significantly lower in the HG+CLZ-8 group ($P < 0.05$). ROS levels in the HG+CLZ-8+Ipatasertib group were significantly higher than those in the HG+CLZ-8 group ($P < 0.05$).

Mitochondrial membrane potential detection results (Fig. 9G, 9H) showed that the membrane potential level in the HG group was significantly lower than that in the Control group ($P < 0.05$), Ipatasertib further decreased the membrane potential ($P < 0.05$), while CLZ-8 intervention significantly increased the membrane potential level in the HG+CLZ-8 group ($P < 0.05$).

Tunel kit was used to detect apoptosis (Fig. 9I, 9J). There were few apoptotic cells in the Control group, and no significant difference between the HG group and the Control group. The number of apoptotic cells in the HG+Ipatasertib group was significantly higher than that in the HG group ($P < 0.05$), while the number of apoptotic cells in the HG+CLZ-8 group was significantly lower than that in the HG group ($P < 0.05$). These results indicate that Sodium selenite can upregulate SelH expression. SelH overexpression itself has limited effects on inhibiting ROS production and protecting mitochondrial membrane potential, suggesting that the protective effect of SelH is achieved through regulating the p53/PUMA apoptotic pathway rather than reducing oxidative stress.

3.10. SelH overexpression reduces HT22 cell apoptosis by inhibiting p53/puma and increasing the bcl-2/Bax ratio in vitro

p53/puma immunofluorescence (Fig. 10A, 10B, and 10C) and bcl-2 and Bax immunofluorescence (Fig. 10D, 10E) were used to observe the apoptosis of SelH-overexpressing cells. In the Control group, the expressions of p53 and puma were low, and the bcl-2/Bax ratio was low. In the HG group, the expressions of p53 and puma were increased to a certain extent compared with the Control group ($P < 0.05$), and there was no statistical difference in the expression of bcl-2/Bax compared with the Control group. After Ipatasertib intervention, the expressions of p53 and puma were further increased ($P < 0.05$), and the bcl-2/Bax ratio was further decreased ($P < 0.05$) in the HG+Ipatasertib group. In contrast, after CLZ-8 intervention, the expressions of p53 and puma were significantly decreased ($P < 0.05$), and the bcl-2/Bax ratio was significantly increased ($P < 0.05$) in the HG+CLZ-8 group. This indicates that SelH overexpression can reduce the decrease in p53 and puma expressions and the decrease in the bcl-2/Bax ratio caused by high glucose-OGD/R, protect cell status, and reduce apoptosis.

4. Discussion

Under hyperglycemic conditions, cerebral I/R injury is significantly exacerbated. In animal models, hyperglycemic rats exhibit severe neurological deficits, significantly enlarged cerebral infarct volume, and histomorphological damage. In cell models, Sodium selenite not only improves the decreased viability of HT22 cells in the high glucose-oxygen deprivation group. Studies have confirmed that selenium can effectively alleviate cerebral I/R injury under hyperglycemic conditions [22]. In our study, the Sodium selenite intervention group indeed improved the neurological function score, reduced the infarct volume, and alleviated brain tissue damage in hyperglycemic rats. Sodium selenite improved the decreased viability of high glucose-HT22 cells, thereby verifying the protective effect of selenium against cerebral ischemic injury under hyperglycemic conditions.

The pathological mechanism of hyperglycemia combined with cerebral I/R injury is complex, involving a complex regulatory network of energy metabolism disorders [30], oxidative stress [31,32], inflammatory cascade reactions [33,34], apoptosis [35], and ferroptosis [36]. Previous studies have reported that chronic hyperglycemia induces the activation of advanced glycation end products (AGEs) and RAGE receptors, exacerbating blood-brain barrier damage and neuroinflammatory responses [37]. This study innovatively designed a bidirectional control research paradigm to systematically compare the spatiotemporal differential pathological changes in the cortex and medulla of ischemic and non-ischemic brain tissues during the acute phase (24h) and recovery phase (72h) of reperfusion. Increased proportion of nuclear pyknosis and discretization of Nissl bodies were observed in both ischemic and non-ischemic brain tissues after hyperglycemic cerebral ischemia. These results confirm the global damage effect of AGEs, providing new evidence for clarifying the spatiotemporal-specific mechanism by which hyperglycemia aggravates cerebral I/R injury. Secondly, in the hyperglycemic environment, intracellular metabolism is disrupted, NADH/FADH supply is significantly increased, leading to excessive load on the mitochondrial electron transport chain, thereby triggering explosive accumulation of reactive

oxygen species (ROS) [38]. Hyperglycemia can also activate the protein kinase C (PKC) pathway, enhance NADPH oxidase activity, and further amplify ROS burst [39]. In this study, ROS production was significantly increased in the high glucose culture group compared with the normal glucose culture group in HT22 cell, providing supplementary evidence for this mechanism. Excessive ROS have strong oxidizing properties and can cause severe damage to mitochondrial structure and function. In this study, transmission electron microscopy results showed that mitochondrial cristae disappeared and vacuolization occurred in nerve cells after hyperglycemic cerebral ischemia, and mitochondrial membrane potential decreased. The decrease in mitochondrial membrane potential is an early event of apoptosis, reflecting the loss of inner mitochondrial membrane integrity and ATP synthesis disorders [40]. In addition, impaired autophagic flux caused by diabetes leads to the accumulation of abnormal proteins, weakening the ability of neurons to clear ischemic damage [41]. These mechanisms interact to form a cascade reaction network of diabetic cerebral ischemic injury. Sodium selenite intervention can effectively antagonize the neuroinjury cascade induced by high glucose metabolism disorders, protect brain tissue, and alleviate hyperglycemia-aggravated cerebral I/R injury.

Accumulation of ROS in the hyperglycemic cerebral ischemic environment directly activates the p53/puma apoptotic axis [42]. Elmore S et al. first discovered the specific activation of p53 in diabetic cerebral ischemia [42]. Similarly, in this study, the p-p53/p53 ratio was significantly increased in the hyperglycemic I/R 24h group, and the expression of puma, a key downstream effector molecule of p53, was also significantly increased, driving Bax translocation to mitochondria, inducing increased mitochondrial outer membrane permeability, releasing cytochrome c, and activating the caspase-9/3 cascade reaction. In HT22 cells, after high glucose OGD/R, ROS levels were significantly increased, mitochondrial membrane potential was decreased, the proportion of Tunel-positive cells was increased, and the expressions of apoptotic factors such as p53, puma, and caspase 3 were increased. Mitochondrial damage further exacerbates ROS release, forming a positive feedback loop of "ROS-p53-puma-mitochondrial damage-ROS", which becomes the core mechanism by which hyperglycemia aggravates cerebral ischemic injury. In this study, Sodium selenite blocks this cycle by scavenging ROS, thereby alleviating hyperglycemia-aggravated cerebral I/R injury.

In cerebral I/R injury and other diseases, puma, as a pro-apoptotic protein downstream of p53, induces cell apoptosis through the mitochondrial pathway [43-48]. This study found that the high glucose environment significantly exacerbates the upregulation of puma expression induced by I/R or OGD/R, and further amplifies its pro-apoptotic effect by activating p53 phosphorylation (increased p-p53/p53 ratio), while Sodium selenite treatment can significantly inhibit the expressions of both. Notably, puma downregulation not only reduces its own protein level but also unexpectedly inhibits p53 expression and phosphorylation, suggesting a possible bidirectional regulatory relationship between them. This finding updates the traditional understanding of the "p53 regulates puma" unidirectional pathway. A possible mechanism is that mitochondrial damage caused by hyperglycemic cerebral ischemia leads to increased ROS production during puma-mediated cell apoptosis, thereby affecting p53 expression [49]. The pro-apoptotic effect of puma is mainly reflected in the activation of the mitochondrial pathway [50]. Its upregulation leads to a significant decrease in the bcl-2/Bax ratio, promoting mitochondrial membrane

potential collapse. These results reveal the dual destructive effect of the high glucose environment on mitochondrial homeostasis through enhancing the p53/puma pathway, which not only exacerbates ROS burst but also accelerates energy metabolism failure through membrane potential hyperpolarization. Sodium selenite blocks this process by inhibiting puma expression, providing a new explanation for the specific injury mechanism in patients with diabetes mellitus complicated with cerebral ischemia.

Sodium selenite, as a biologically active form of selenium, has dual roles in regulating redox homeostasis and apoptotic signals. The biological functions of Sodium selenite are mainly achieved through selenoproteins, which play a core role in the antioxidant defense system. The brain is highly dependent on selenium to maintain neural function. Selenoprotein P, GPX4, and selenoprotein W are the most abundantly expressed selenoproteins in the central nervous system [51]. Glutathione peroxidases (GPX1-4) can efficiently scavenge peroxides [52], and selenoprotein K, selenoprotein P, etc., regulate redox balance through selenocysteine residues [53]. Studies have shown that Sodium selenite pretreatment improves cerebral infarction volume, reduces DNA oxidation, and protects glutamate-induced hippocampal HT22 neuronal cells [54]. Recent studies have found that Sodium selenite induces apoptosis of cervical cancer cells through the mitochondrial ROS-activated AMPK/mTOR/FOXO3a pathway [55]. Combined with in vivo and in vitro models, this study found that Sodium selenite can improve the neurological function score, reduce the infarct volume of hyperglycemic rats, improve the decreased viability of high glucose-HT22 cells, reduce ROS production, increase mitochondrial membrane potential, reduce apoptosis, and protect against cerebral ischemic injury under hyperglycemic conditions.

As a nuclear selenoprotein, SelH directly binds to DNA through the KUGU domain. Under oxidative stress, it can activate the Nrf2/ARE pathway to enhance the expression of antioxidant enzymes and participate in DNA damage repair [56,57]. In the results of this study, supplementation with Sodium selenite can increase SelH expression. In the SelH-overexpressing HT22 cell model, the expressions of pro-apoptotic proteins such as puma and p-p53/p53 were significantly decreased, while the expression of the anti-apoptotic protein bcl-2 and the bcl-2/Bax ratio were increased. This study also found that SelH overexpression did not inhibit ROS or protect mitochondrial membrane potential, indicating that the protective effect of SelH is achieved through regulating the p53/PUMA apoptotic pathway rather than reducing oxidative stress. It is suggested that Sodium selenite may reduce oxidative stress through other selenoproteins or other mechanisms, which may be related to the enhanced selenium-dependent GPX activity [58]. Notably, the protective effect of SelH may be puma-dependent. The puma activator Ipatasertib can completely offset the protective effect of SelH by upregulating puma. This is consistent with the research by Regina Brigelius-Flohé et al., which concluded that normal selenium intake inhibits oxidation-driven programmed cell death cascades by eliminating death signals and inhibits hydrogen peroxide-induced inflammatory cascades [59-60]. Therefore, the breakthrough of this study is to clarify the specific role of the SelH-puma axis in hyperglycemic cerebral ischemia, providing a theoretical basis for the development of SelH-targeted neuroprotective agents for diabetes mellitus.

In summary, this study systematically reveals the cascade reaction network of cerebral I/R injury under diabetic hyperglycemic conditions, and innovatively clarifies the molecular mechanism by which Sodium selenite exerts neuroprotective effects through the SelH-puma axis. This not only provides a new perspective for understanding diabetes-related neurological complications but also lays an experimental foundation for the development of puma-targeted selenium-based neuroprotective agents, with significant clinical transformation potential.

The significant correlation between puma expression and cerebral infarct volume suggests that it can be used as a prognostic biomarker for diabetic stroke. Dynamic monitoring of its level changes helps evaluate the degree of brain injury and prognosis. In terms of treatment strategies, administration of Sodium selenite in the acute phase can effectively block the "puma-ROS" positive feedback loop, providing a key time window reference for clinical treatment. Meanwhile, the development of small molecule inhibitors targeting puma (such as CLZ-8) and SelH agonists has potential therapeutic value and may become neuroprotective agents for patients with diabetic cerebral ischemia. The synergistic therapeutic strategy of puma knockout combined with Sodium selenite significantly reduces the apoptotic rate and improves the neurological function score, providing a new combined treatment idea for clinical practice. However, this study still has limitations. The specific molecular mechanism by which SelH regulates puma (such as transcriptional or post-transcriptional regulation) has not been fully elucidated, and further exploration in transgenic animal models is needed in the future.

Declarations

Funding

This research was supported by the Shanghai Key Laboratory of Forensic Medicine and Key Laboratory of Forensic Science, Ministry of Justice (No. KF202501), the National Natural Science Foundation of China (No. 82260253), the Natural Science Foundation of Ningxia (No. 2024AAC03249), 2023 Ningxia Hui Autonomous Region Youth Science and Technology Promotion Talent Training Project (LY).

Author Contribution

Tianxiang Zheng performed the experiments, conducted data analysis. Xida Yin and Feng Ding participated in the experimental procedures and prepared the initial draft of the manuscript. Shuai Zhao, Yajuan Fu and Yue Chang offered technical assistance and conducted the statistical analysis. Zhiyao Lian, Xinyan Zhao and Li Jing conducted data analysis and was responsible for animal feeding. Lan Yang contributed to the design of the experimental study, provided funding, and finalized the article. All authors reviewed and approved the final manuscript and gave their consent for the submitted version.

Data Availability

Data will be made available on request.

Ethics Approval and Consent to Participate All animal procedures are conducted by the NIH Guide for the Care and Use of Laboratory Animals and approved by the Institutional Animal Care and Use Committee of Ningxia Medical University (IACUC-NYLAC-2023-038).

Consent for Publication Not applicable.

Competing Interests The authors declare no competing interests.

Declaration of clinical trial number Not applicable.

References

1. Bitter, I., Szekeres, G., Cai, Q., Feher, L., Gimesi-Orszagh, J., Kunovszki, P., El Khoury, A. C., Dome, P., & Rihmer, Z. (2024). Mortality in patients with major depressive disorder: A nationwide population-based cohort study with 11-year follow-up. European psychiatry : the journal of the Association of European Psychiatrists, 67(1), e63. https://doi.org/10.1192/j.eurpsy.2024.1771
2. Steliga, A., Kowiański, P., Czuba, E., Waśkow, M., Moryś, J., & Lietzau, G. (2020). Neurovascular Unit as a Source of Ischemic Stroke Biomarkers-Limitations of Experimental Studies and Perspectives for Clinical Application. Translational stroke research, 11(4), 553–579. https://doi.org/10.1007/s12975-019-00744-5
3. Dupré, N., Arabo, A., Orset, C., Maucotel, J., Detroussel, Y., Hauchecorne, M., Gonzalez, B. J., Marret, S., Vivien, D., & Leroux, P. (2020). Neonatal cerebral hypoxia-ischemia in mice triggers age-dependent vascular effects and disabilities in adults; implication of tissue plasminogen activator (tPA). Experimental neurology, 323, 113087. https://doi.org/10.1016/j.expneurol.2019.113087
4. Misra, S., Khan, E. I., Lam, T. T., Mazumder, R., Gururangan, K., Hickman, L. B., Goswami, V., Funaro, M. C., Eldem, E., Sansing, L. H., Sico, J. J., Quinn, T. J., Liebeskind, D. S., Montaner, J., Kwan, P., & Mishra, N. K. (2023). Common Pathways of Epileptogenesis in Patients With Epilepsy Post-Brain Injury: Findings From a Systematic Review and Meta-analysis. Neurology, 101(22), e2243–e2256. https://doi.org/10.1212/WNL.0000000000207749
5. Mao, R., Zong, N., Hu, Y., Chen, Y., & Xu, Y. (2022). Neuronal Death Mechanisms and Therapeutic Strategy in Ischemic Stroke. Neuroscience bulletin, 38(10), 1229–1247. https://doi.org/10.1007/s12264-022-00859-0
6. Ya, J., Pellumbaj, J., Hashmat, A., & Bayraktutan, U. (2024). The Role of Stem Cells as Therapeutics for Ischaemic Stroke. Cells, 13(2), 112. https://doi.org/10.3390/cells13020112
7. Zeng, J., Bao, T., Yang, K., Zhu, X., Wang, S., Xiang, W., Ge, A., Zeng, L., & Ge, J. (2023). The mechanism of microglia-mediated immune inflammation in ischemic stroke and the role of natural botanical components in regulating microglia: A review. Frontiers in immunology, 13, 1047550. https://doi.org/10.3389/fimmu.2022.1047550
8. Xu, S., Lu, J., Shao, A., Zhang, J. H., & Zhang, J. (2020). Glial Cells: Role of the Immune Response in Ischemic Stroke. Frontiers in immunology, 11, 294. https://doi.org/10.3389/fimmu.2020.00294

9. Li, P., Stetler, R. A., Leak, R. K., Shi, Y., Li, Y., Yu, W., Bennett, M. V. L., & Chen, J. (2018). Oxidative stress and DNA damage after cerebral ischemia: Potential therapeutic targets to repair the genome and improve stroke recovery. Neuropharmacology, 134(Pt B), 208–217. https://doi.org/10.1016/j.neuropharm.2017.11.011
10. Zhang, L., Han, Y., Wu, X., Chen, B., Liu, S., Huang, J., Kong, L., Wang, G., & Ye, Z. (2023). Research progress on the mechanism of curcumin in cerebral ischemia/reperfusion injury: a narrative review. Apoptosis : an international journal on programmed cell death, 28(9-10), 1285–1303. https://doi.org/10.1007/s10495-023-01869-7
11. Burk, R. F., Hill, K. E., & Motley, A. K. (2003). Selenoprotein metabolism and function: evidence for more than one function for selenoprotein P. The Journal of nutrition, 133(5 Suppl 1), 1517S–20S. https://doi.org/10.1093/jn/133.5.1517S
12. Li, L., Wang, M., Ma, Y. M., Yang, L., Zhang, D. H., Guo, F. Y., Jing, L., & Zhang, J. Z. (2023). Selenium inhibits ferroptosis in hyperglycemic cerebral ischemia/reperfusion injury by stimulating the Hippo pathway. PloS one, 18(9), e0291192. https://doi.org/10.1371/journal.pone.0291192
13. Wang, J., Thomas, H. R., Li, Z., Yeo, N. C. F., Scott, H. E., Dang, N., Hossain, M. I., Andrabi, S. A., & Parant, J. M. (2021). Puma, noxa, p53, and p63 differentially mediate stress pathway induced apoptosis. Cell death & disease, 12(7), 659. https://doi.org/10.1038/s41419-021-03902-6
14. Rozenberg, J. M., Zvereva, S., Dalina, A., Blatov, I., Zubarev, I., Luppov, D., Bessmertnyi, A., Romanishin, A., Alsoulaiman, L., Kumeiko, V., Kagansky, A., Melino, G., Ganini, C., & Barlev, N. A. (2021). The p53 family member p73 in the regulation of cell stress response. Biology direct, 16(1), 23. https://doi.org/10.1186/s13062-021-00307-5.
15. Ma, Y. M., Ibeanu, G., Wang, L. Y., Zhang, J. Z., Chang, Y., Dong, J. D., Li, P. A., & Jing, L. (2017). Selenium suppresses glutamate-induced cell death and prevents mitochondrial morphological dynamic alterations in hippocampal HT22 neuronal cells. BMC neuroscience, 18(1), 15. https://doi.org/10.1186/s12868-017-0337-4
16. Wang, Y. J., Li, Z. X., Gu, H. Q., Zhai, Y., Zhou, Q., Jiang, Y., Zhao, X. Q., Wang, Y. L., Yang, X., Wang, C. J., Meng, X., Li, H., Liu, L. P., Jing, J., Wu, J., Xu, A. D., Dong, Q., Wang, D., Wang, W. Z., Ma, X. D., … China Stroke Statistics Writing Committee (2022). China Stroke Statistics: an update on the 2019 report from the National Center for Healthcare Quality Management in Neurological Diseases, China National Clinical Research Center for Neurological Diseases, the Chinese Stroke Association, National Center for Chronic and Non-communicable Disease Control and Prevention, Chinese Center for Disease Control and Prevention and Institute for Global Neuroscience and Stroke Collaborations. Stroke and vascular neurology, 7(5), 415–450. https://doi.org/10.1136/svn-2021-001374
17. Kang, J. B., Kim, D. K., Park, D. J., Shah, M. A., Kim, M. O., Jung, E. J., Lee, H. S., & Koh, P. O. (2018). Hyperglycemia aggravates decrease in alpha-synuclein expression in a middle cerebral artery occlusion model. Laboratory animal research, 34(4), 195–202. https://doi.org/10.5625/lar.2018.34.4.195

18. Lebrun, F., Levard, D., Lemarchand, E., Yetim, M., Furon, J., Potzeha, F., Marie, P., Lesept, F., Blanc, M., Haelewyn, B., Rubio, M., Letourneur, A., Violle, N., Orset, C., & Vivien, D. (2024). Improving stroke outcomes in hyperglycemic mice by modulating tPA/NMDAR signaling to reduce inflammation and hemorrhages. Blood advances, 8(5), 1330–1344. https://doi.org/10.1182/bloodadvances.2023011744
19. Tomas-Sanchez, C., Blanco-Alvarez, V. M., Gonzalez-Barrios, J. A., Martinez-Fong, D., Soto-Rodriguez, G., Brambila, E., Gonzalez-Vazquez, A., Aguilar-Peralta, A. K., Limón, D. I., Vargas-Castro, V., Cebada, J., Alatriste-Bueno, V., & Leon-Chavez, B. A. (2024). Prophylactic zinc and therapeutic selenium administration in adult rats prevents long-term cognitive and behavioral sequelae by a transient ischemic attack. Heliyon, 10(9), e30017. https://doi.org/10.1016/j.heliyon.2024.e30017
20. Mojadadi, A., Au, A., Salah, W., Witting, P., & Ahmad, G. (2021). Role for Selenium in Metabolic Homeostasis and Human Reproduction. Nutrients, 13(9), 3256. https://doi.org/10.3390/nu13093256
21. Schwarz, M., Löser, A., Cheng, Q., Wichmann-Costaganna, M., Schädel, P., Werz, O., Arnér, E. S., & Kipp, A. P. (2023). Side-by-side comparison of recombinant human glutathione peroxidases identifies overlapping substrate specificities for soluble hydroperoxides. Redox biology, 59, 102593. https://doi.org/10.1016/j.redox.2022.102593
22. Yang, L., Ma, Y. M., Shen, X. L., Fan, Y. C., Zhang, J. Z., Li, P. A., & Jing, L. (2020). The Involvement of Mitochondrial Biogenesis in Selenium Reduced Hyperglycemia-Aggravated Cerebral Ischemia Injury. Neurochemical research, 45(8), 1888–1901. https://doi.org/10.1007/s11064-020-03055-6
23. Ren, X., Wang, S., Zhang, C., Hu, X., Zhou, L., Li, Y., & Xu, L. (2020). Selenium ameliorates cadmium-induced mouse leydig TM3 cell apoptosis via inhibiting the ROS/JNK /c-jun signaling pathway. Ecotoxicology and environmental safety, 192, 110266. https://doi.org/10.1016/j.ecoenv.2020.110266
24. Wang, S., Chen, Y., Han, S., Liu, Y., Gao, J., Huang, Y., Sun, W., Wang, J., Wang, C., & Zhao, J. (2022). Selenium nanoparticles alleviate ischemia reperfusion injury-induced acute kidney injury by modulating GPx-1/NLRP3/Caspase-1 pathway. Theranostics, 12(8), 3882–3895. https://doi.org/10.7150/thno.70830
25. Turovsky, E. A., Plotnikov, E. Y., & Varlamova, E. G. (2024). Regulatory Role and Cytoprotective Effects of Exogenous Recombinant SELENOM under Ischemia-like Conditions and Glutamate Excitotoxicity in Cortical Cells In Vitro. Biomedicines, 12(8), 1756. https://doi.org/10.3390/biomedicines12081756
26. Plummer, J. D., Postnikoff, S. D., Tyler, J. K., & Johnson, J. E. (2021). Selenium supplementation inhibits IGF-1 signaling and confers methionine restriction-like healthspan benefits to mice. eLife, 10, e62483. https://doi.org/10.7554/eLife.62483
27. Chen, X., & Zhang, X. (2022). Effect of prior exposure to enriched environment on cellular apoptosis after experimental stroke. Molecular biology reports, 49(7), 6541–6551. https://doi.org/10.1007/s11033-022-07494-y

28. Liu, W., Miao, Y., Zhang, L., Xu, X., & Luan, Q. (2020). MiR-211 protects cerebral ischemia/reperfusion injury by inhibiting cell apoptosis. Bioengineered, 11(1), 189–200. https://doi.org/10.1080/21655979.2020.1729322
29. Ma, N., Luo, X., Wang, J., Sun, S., Liang, R., Zhang, Z., Cheng, Z., Wang, J., & Ma, Y. (2025). Inner Mitochondrial Membrane Peptidase 2-Like Deletion Aggravates Mitochondrial Apoptosis and Inhibits Autophagy After Hyperglycemia Stroke. Molecular neurobiology, 62(6), 6884–6897. https://doi.org/10.1007/s12035-024-04479-9
30. Martynov, M. Y., Zhuravleva, M. V., Vasyukova, N. S., Kuznetsova, E. V., & Kameneva, T. R. (2023). Okislitel'nyi stress v patogeneze tserebral'nogo insul'ta i ego korrektsiya [Oxidative stress in the pathogenesis of stroke and its correction]. Zhurnal nevrologii i psikhiatrii imeni S.S. Korsakova, 123(1), 16–27. https://doi.org/10.17116/jnevro202312301116
31. Koutsaliaris, I. K., Moschonas, I. C., Pechlivani, L. M., Tsouka, A. N., & Tselepis, A. D. (2022). Inflammation, Oxidative Stress, Vascular Aging and Atherosclerotic Ischemic Stroke. Current medicinal chemistry, 29(34), 5496–5509. https://doi.org/10.2174/0929867328666210921161711
32. Zhang, Y., Chen, Q., Chen, D., Zhao, W., Wang, H., Yang, M., Xiang, Z., & Yuan, H. (2022). SerpinA3N attenuates ischemic stroke injury by reducing apoptosis and neuroinflammation. CNS neuroscience & therapeutics, 28(4), 566–579. https://doi.org/10.1111/cns.13776
33. Guo, J., Tuo, Q. Z., & Lei, P. (2023). Iron, ferroptosis, and ischemic stroke. Journal of neurochemistry, 165(4), 487–520. https://doi.org/10.1111/jnc.15807
34. Shen, J., Zhang, P., Li, Y., Fan, C., Lan, T., Wang, W., & Yu, S. Y. (2021). Neuroprotective effects of microRNA-211-5p on chronic stress-induced neuronal apoptosis and depression-like behaviours. Journal of cellular and molecular medicine, 25(14), 7028–7038. https://doi.org/10.1111/jcmm.16716
35. Zhu, J., Ji, X., Shi, R., He, T., Chen, S. Y., Cong, R., He, B., Liu, S., Xu, H., & Gu, J. H. (2023). Hyperglycemia Aggravates the Cerebral Ischemia Injury via Protein O-GlcNAcylation. Journal of Alzheimer's disease : JAD, 94(2), 651–668. https://doi.org/10.3233/JAD-230264
36. Guo, Y., Jiang, H., Wang, M., Ma, Y., Zhang, J., & Jing, L. (2023). Metformin alleviates cerebral ischemia/reperfusion injury aggravated by hyperglycemia via regulating AMPK/ULK1/PINK1/Parkin pathway-mediated mitophagy and apoptosis. Chemico-biological interactions, 384, 110723. https://doi.org/10.1016/j.cbi.2023.110723
37. He, J., Liu, J., Huang, Y., Tang, X., Xiao, H., & Hu, Z. (2021). Oxidative Stress, Inflammation, and Autophagy: Potential Targets of Mesenchymal Stem Cells-Based Therapies in Ischemic Stroke. Frontiers in neuroscience, 15, 641157. https://doi.org/10.3389/fnins.2021.641157
38. Li, M., Meng, Z., Yu, S., Li, J., Wang, Y., Yang, W., & Wu, H. (2022). Baicalein ameliorates cerebral ischemia-reperfusion injury by inhibiting ferroptosis via regulating GPX4/ACSL4/ACSL3 axis. Chemico-biological interactions, 366, 110137. https://doi.org/10.1016/j.cbi.2022.110137
39. Lee, T. L., Lai, T. C., Lin, S. R., Lin, S. W., Chen, Y. C., Pu, C. M., Lee, I. T., Tsai, J. S., Lee, C. W., & Chen, Y. L. (2021). Conditioned medium from adipose-derived stem cells attenuates ischemia/reperfusion-

induced cardiac injury through the microRNA-221/222/PUMA/ETS-1 pathway. Theranostics, 11(7), 3131–3149. https://doi.org/10.7150/thno.52677

40. Zhang, Z., Zhang, H., Li, D., Zhou, X., Qin, Q., & Zhang, Q. (2021). Caspase-3-mediated GSDME induced Pyroptosis in breast cancer cells through the ROS/JNK signalling pathway. Journal of cellular and molecular medicine, 25(17), 8159–8168. https://doi.org/10.1111/jcmm.16574
41. Li M. (2021). The role of P53 up-regulated modulator of apoptosis (PUMA) in ovarian development, cardiovascular and neurodegenerative diseases. Apoptosis : an international journal on programmed cell death, 26(5-6), 235–247. https://doi.org/10.1007/s10495-021-01667-z
42. Elmore S. (2007). Apoptosis: a review of programmed cell death. Toxicologic pathology, 35(4), 495–516. https://doi.org/10.1080/01926230701320337
43. Roufayel, R., Younes, K., Al-Sabi, A., & Murshid, N. (2022). BH3-Only Proteins Noxa and Puma Are Key Regulators of Induced Apoptosis. Life (Basel, Switzerland), 12(2), 256. https://doi.org/10.3390/life12020256
44. Tanaka, K., Yu, H. A., Yang, S., Han, S., Selcuklu, S. D., Kim, K., Ramani, S., Ganesan, Y. T., Moyer, A., Sinha, S., Xie, Y., Ishizawa, K., Osmanbeyoglu, H. U., Lyu, Y., Roper, N., Guha, U., Rudin, C. M., Kris, M. G., Hsieh, J. J., & Cheng, E. H. (2021). Targeting Aurora B kinase prevents and overcomes resistance to EGFR inhibitors in lung cancer by enhancing BIM- and PUMA-mediated apoptosis. Cancer cell, 39(9), 1245–1261.e6. https://doi.org/10.1016/j.ccell.2021.07.006
45. Tao, X., Zhang, G., Liu, J., Ji, B., Xu, H., & Chen, Z. (2022). PATZ1 Induces Apoptosis through PUMA in Glioblastoma. Journal of oncology, 2022, 4953107. https://doi.org/10.1155/2022/4953107
46. Sabapathy, K., & Lane, D. P. (2019). Understanding p53 functions through p53 antibodies. Journal of molecular cell biology, 11(4), 317–329. https://doi.org/10.1093/jmcb/mjz010
47. Yu, J., & Zhang, L. (2003). No PUMA, no death: implications for p53-dependent apoptosis. Cancer cell, 4(4), 248–249. https://doi.org/10.1016/s1535-6108(03)00249-6
48. Rog, J., Łobejko, Ł., Hordejuk, M., Marciniak, W., Derkacz, R., Kiljańczyk, A., Matuszczak, M., Lubiński, J., Nesterowicz, M., Żendzian-Piotrowska, M., Zalewska, A., Maciejczyk, M., & Karakula-Juchnowicz, H. (2024). Pro/antioxidant status and selenium, zinc and arsenic concentration in patients with bipolar disorder treated with lithium and valproic acid. Frontiers in molecular neuroscience, 17, 1441575. https://doi.org/10.3389/fnmol.2024.1441575
49. Dardashti, R. N., Laps, S., Gichtin, J. S., & Metanis, N. (2023). The semisynthesis of nucleolar human selenoprotein H. Chemical science, 14(44), 12723–12729. https://doi.org/10.1039/d3sc03059h
50. Maia, L. B., Maiti, B. K., Moura, I., & Moura, J. J. G. (2023). Selenium-More than Just a Fortuitous Sulfur Substitute in Redox Biology. Molecules (Basel, Switzerland), 29(1), 120. https://doi.org/10.3390/molecules29010120
51. Mojadadi, A., Au, A., Salah, W., Witting, P., & Ahmad, G. (2021). Role for Selenium in Metabolic Homeostasis and Human Reproduction. Nutrients, 13(9), 3256. https://doi.org/10.3390/nu13093256

52. Muhammad, A. I., Mohamed, D. A. A., Chwen, L. T., Akit, H., & Samsudin, A. A. (2021). Effect of Sodium Selenite, Selenium Yeast, and Bacterial Enriched Protein on Chicken Egg Yolk Color, Antioxidant Profiles, and Oxidative Stability. Foods (Basel, Switzerland), 10(4), 871. https://doi.org/10.3390/foods10040871
53. Kalimuthu, K., Keerthana, C. K., Mohan, M., Arivalagan, J., Christyraj, J. R. S. S., Firer, M. A., Choudry, M. H. A., Anto, R. J., & Lee, Y. J. (2022). The emerging role of selenium metabolic pathways in cancer: New therapeutic targets for cancer. Journal of cellular biochemistry, 123(3), 532–542. https://doi.org/10.1002/jcb.30196
54. Zhang, Z., He, J., & Wang, B. (2021). Circular RNA circ_HECTD1 regulates cell injury after cerebral infarction by miR-27a-3p/FSTL1 axis. Cell cycle (Georgetown, Tex.), 20(9), 914–926. https://doi.org/10.1080/15384101.2021.1909885
55. Li M. (2021). The role of P53 up-regulated modulator of apoptosis (PUMA) in ovarian development, cardiovascular and neurodegenerative diseases. Apoptosis : an international journal on programmed cell death, 26(5-6), 235–247. https://doi.org/10.1007/s10495-021-01667-z
56. Brigelius-Flohé, R., & Arnér, E. S. J. (2018). Selenium and selenoproteins in (redox) signaling, diseases, and animal models - 200 year anniversary issue. Free radical biology & medicine, 127, 1–2. https://doi.org/10.1016/j.freeradbiomed.2018.09.026
57. Alsulami, F. J., & Shaheed, S. U. (2024). Role of Natural Antioxidants in Cancer. Cancer treatment and research, 191, 95–117. https://doi.org/10.1007/978-3-031-55622-7_4
58. Mao, Z., Tian, L., Liu, J., Wu, Q., Wang, N., Wang, G., Wang, Y., & Seto, S. (2022). Ligustilide ameliorates hippocampal neuronal injury after cerebral ischemia reperfusion through activating PINK1/Parkin-dependent mitophagy. Phytomedicine : international journal of phytotherapy and phytopharmacology, 101, 154111.https://doi.org/10.1016/j.phymed.2022.154111
59. Brigelius-Flohé, R., & Flohé, L. (2017). Selenium and redox signaling. Archives of biochemistry and biophysics, 617, 48–59. https://doi.org/10.1016/j.abb.2016.08.003
60. Brigelius-Flohé, R., & Maiorino, M. (2013). Glutathione peroxidases. Biochimica et biophysica acta, 1830(5), 3289–3303. https://doi.org/10.1016/j.bbagen.2012.11.020

Figures

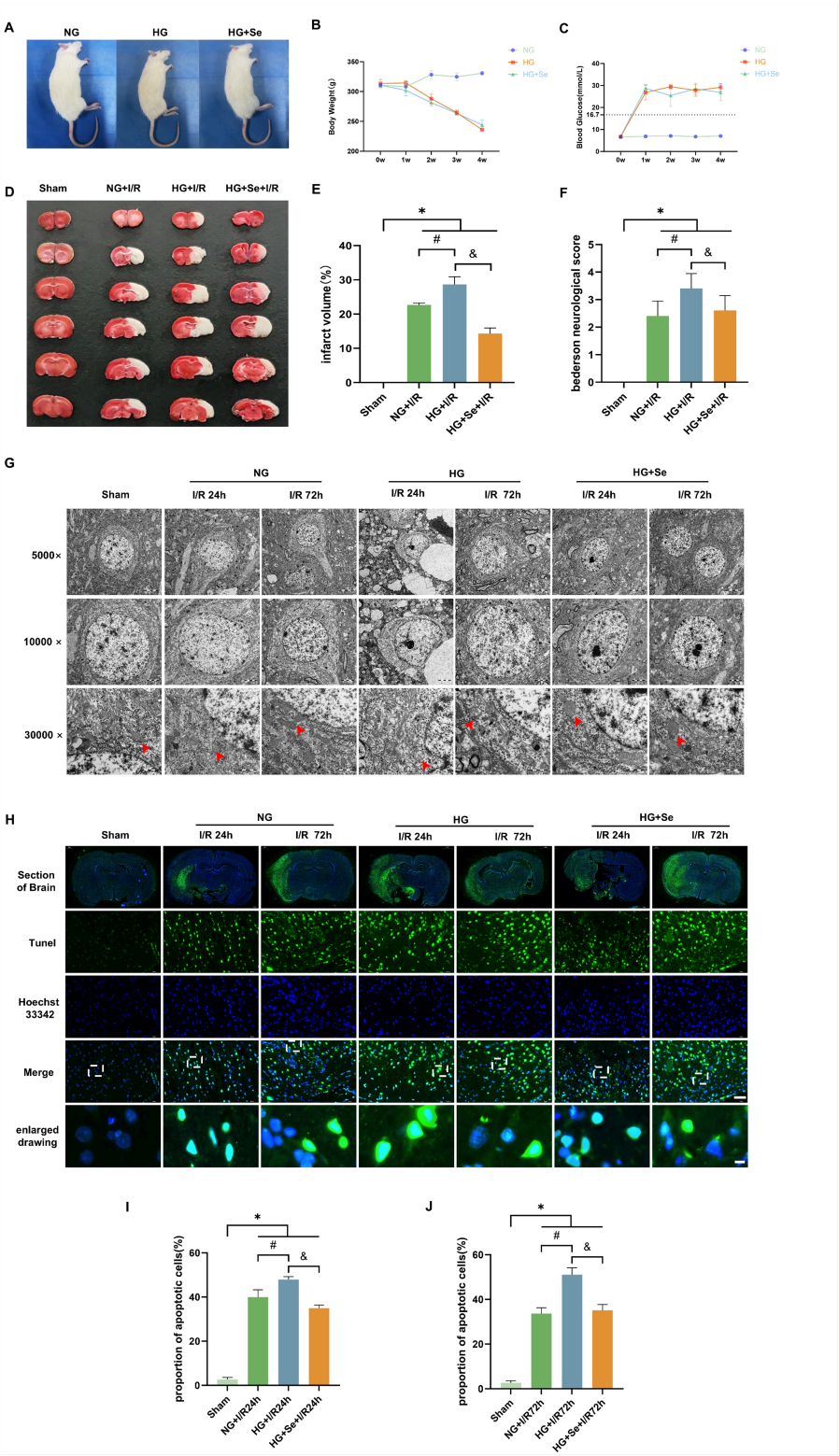


Figure 1

Sodium selenite improves neurological function and tissue damage after hyperglycemia-aggravated cerebral I/R in rats. (A) Representative images of rat posture. (B) Rat body weight change curve. (C) Dynamic monitoring of rat blood glucose levels. (D) Representative images of TTC staining. (E) Statistical analysis of relative infarct volume (n=3). (F) Neurological deficit score. (G) Transmission electron microscopy images of the cortical area in the ischemic penumbra (bar = 10 μm). (H) Tunel

staining images (bar = 50 μm). (I) Statistical analysis of the number of apoptotic neurons at I/R 24 h. (J) Statistical analysis of the number of apoptotic neurons at I/R 72 h. *P < 0.05 vs. Sham; #P < 0.05 vs. NG+I/R; &P < 0.05 vs. HG+I/R

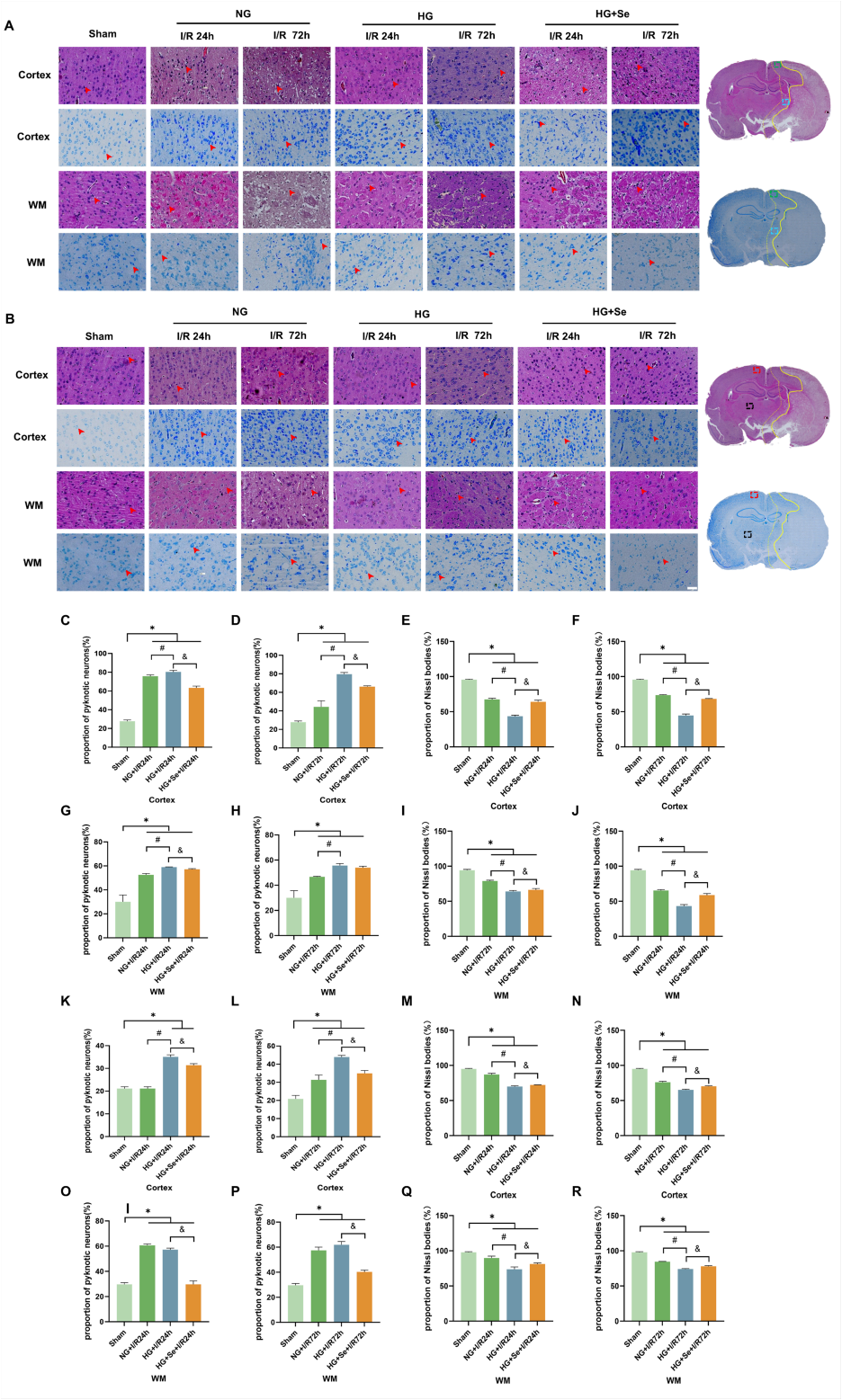


Figure 2

Sodium selenite alleviates histopathological damage of cerebral I/R aggravated by hyperglycemia. (A) HE and Nissl staining of the cortical and medullary areas on the ischemic side (bar = 50 μm). (B) HE and

Nissl staining of the corresponding areas on the contralateral side (bar = 50 μm). (C–J) Statistical analysis of the proportion of pyknotic neurons and the proportion of neurons containing Nissl bodies in the ischemic penumbra. (K–R) Statistical analysis of the proportion of pyknotic neurons and the proportion of neurons containing Nissl bodies in the corresponding contralateral areas. *P < 0.05 vs. Sham; #P < 0.05 vs. NG+I/R; &P < 0.05 vs. HG+I/R

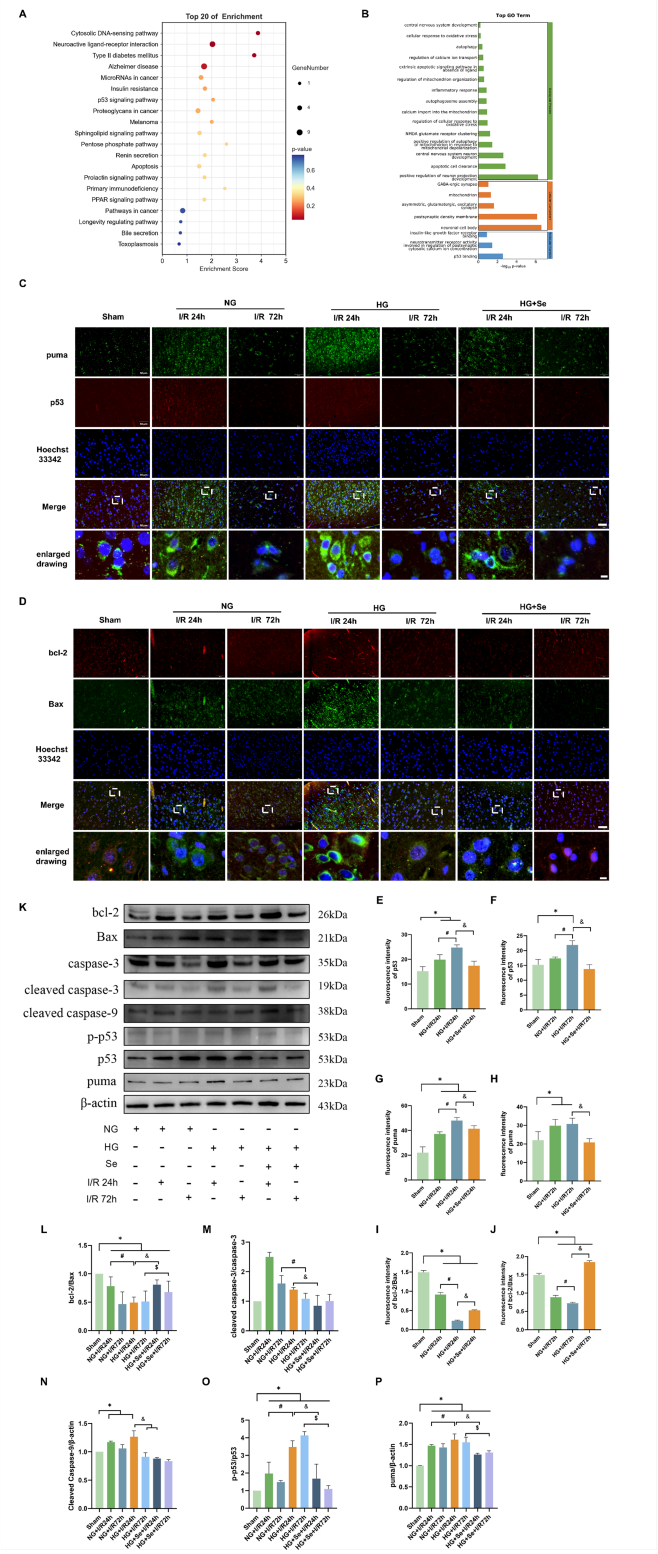


Figure 3

Sodium selenite inhibits hyperglycemia-aggravated neuronal apoptosis via the p53/puma pathway. (A) KEGG pathway enrichment. (B) GO function enrichment. (C) Co-immunofluorescence labeling of p53 and puma in brain tissue (bar = 50 μm, bar = 10 μm). (D) Co-immunofluorescence labeling of bcl-2 and Bax in brain tissue (bar = 50 μm, bar = 10 μm). (E–H) Statistical analysis of relative fluorescence intensities of p53 and puma. (I–J) Statistical analysis of the fluorescence intensity ratio of bcl-2/Bax. (K) Western blot bands. (L–P) Quantitative statistical analysis of corresponding proteins. *P < 0.05 vs. Sham; #P < 0.05 vs. NG+I/R; &P < 0.05 vs. HG+I/R

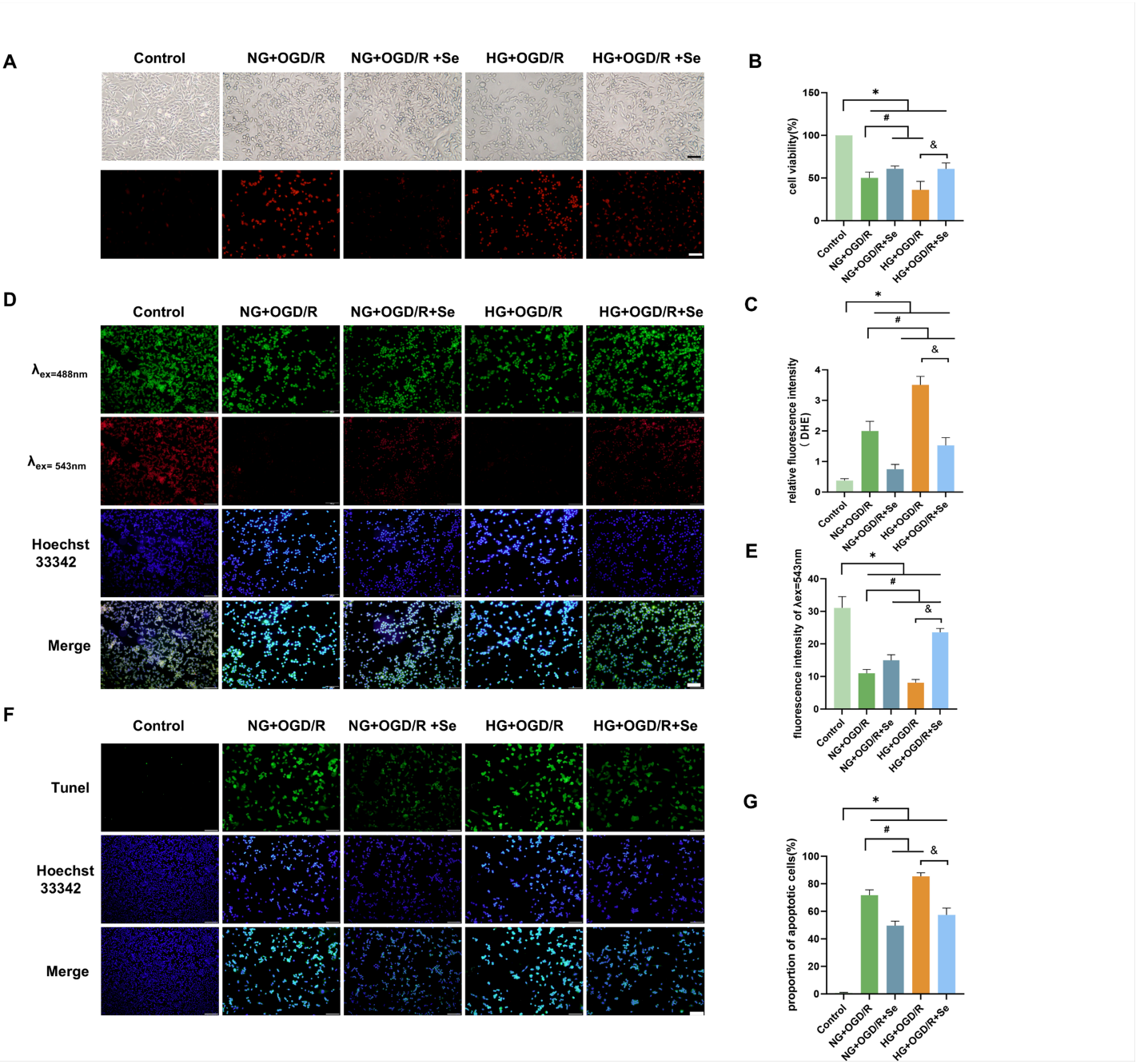


Figure 4

Sodium selenite attenuates high glucose-OGD/R-induced HT22 cell damage. (A) Representative images of cell morphology and ROS (bar = 50 μm). (B) CCK-8 assay for cell viability. (C) Statistical analysis of relative ROS fluorescence intensity. (D) Mitochondrial membrane potential (JC-1) images (bar = 50 μm).

(E) Statistical analysis of the mitochondrial membrane potential (JC-1) ratio. (F) Tunel staining images (bar = 50 μm). (G) Statistical analysis of apoptotic cell ratio. *P < 0.05 vs. Control; #P < 0.05 vs. NG+OGD/R; &P < 0.05 vs. HG+OGD/R

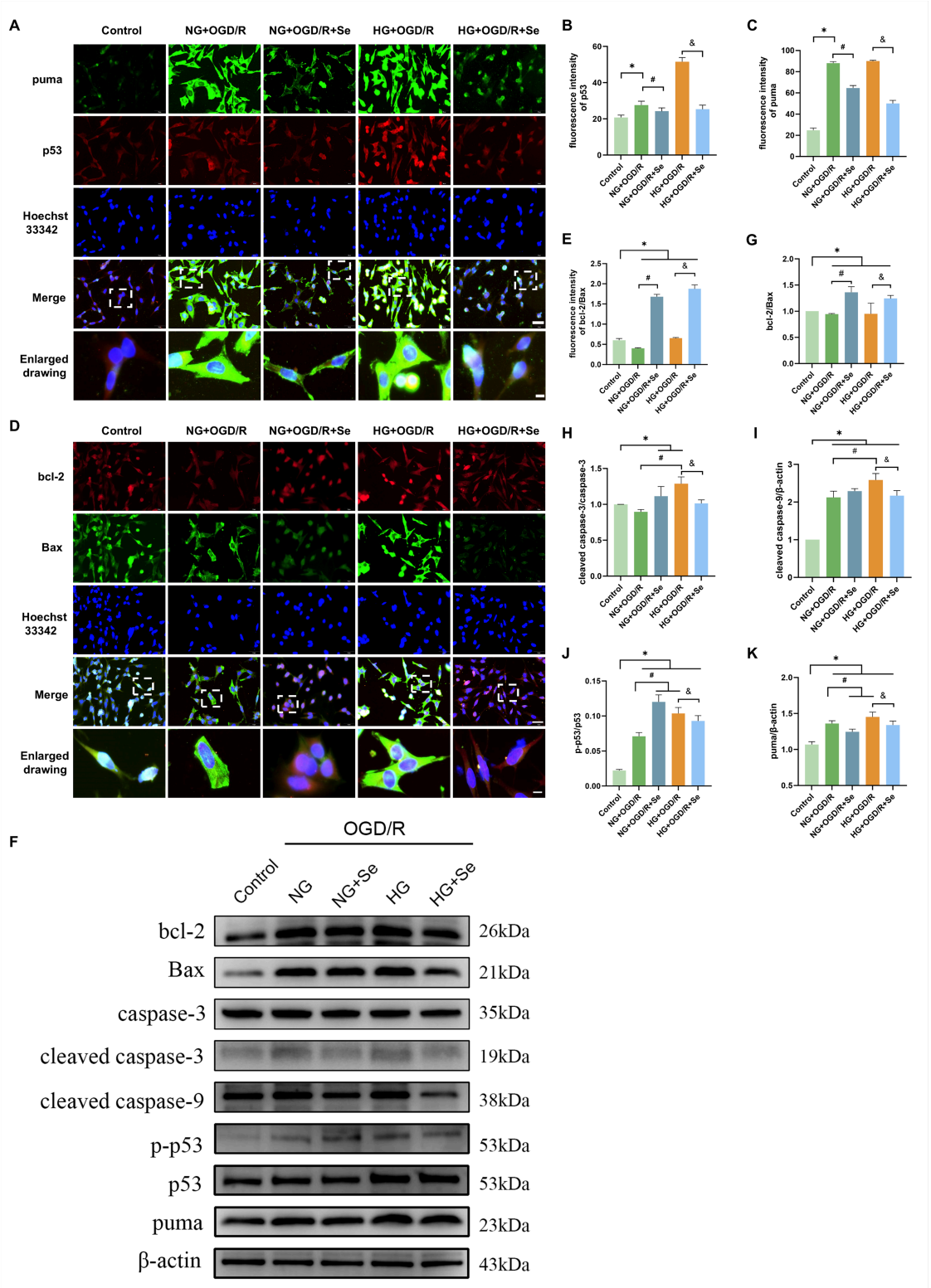


Figure 5

Sodium selenite reduces high glucose-OGD/R-induced cell apoptosis via the p53/puma-bcl-2/Bax axis (A) Double immunofluorescence labeling of p53 and puma (bar = 50 μm, bar = 10 μm). (B–C) Statistical

analysis of fluorescence intensities of p53 and puma. (D) Co-immunofluorescence labeling of bcl-2 and Bax (bar = 50 μm, bar = 10 μm). (E) Statistical analysis of the fluorescence intensity ratio of bcl-2/Bax. (F) Western blot bands. (G–K) Quantitative statistical analysis of apoptosis-related proteins. *P < 0.05 vs. Control; #P < 0.05 vs. NG+OGD/R; &P < 0.05 vs. HG+OGD/R

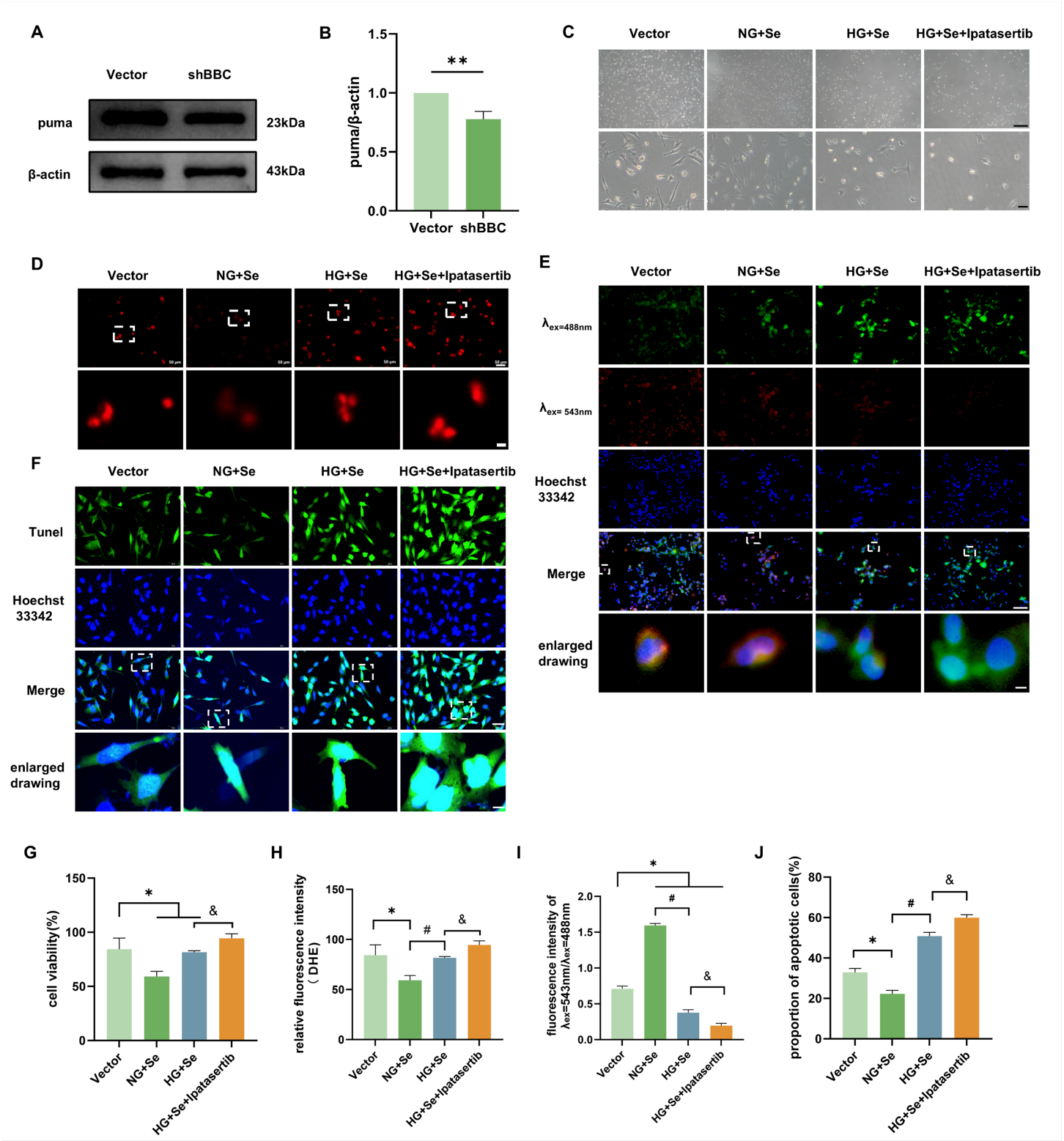


Figure 6

PUMA downregulation attenuates high glucose-OGD/R-induced injury in HT22 cells. (A) Western blot bands of PUMA knockdown. (B) Quantitative analysis of Western blot results. (C) Representative images of cellular morphology (scale bar = 50 μm). (D) Representative images of ROS staining (scale bar = 50 μm). (E) Representative images of JC-1 staining (scale bar = 50 μm). (F) Representative images of TUNEL staining (scale bar = 50 μm). (G) Cell viability detected by CCK-8 assay. (H) Relative fluorescence intensity of ROS. (I) Mitochondrial membrane potential (JC-1) ratio. (J) Quantitative analysis of apoptotic rate. *P < 0.05 vs. Vector group; #P < 0.05 vs. NG+Se+OGD/R group; &P < 0.05 vs. HG+Se+OGD/R group

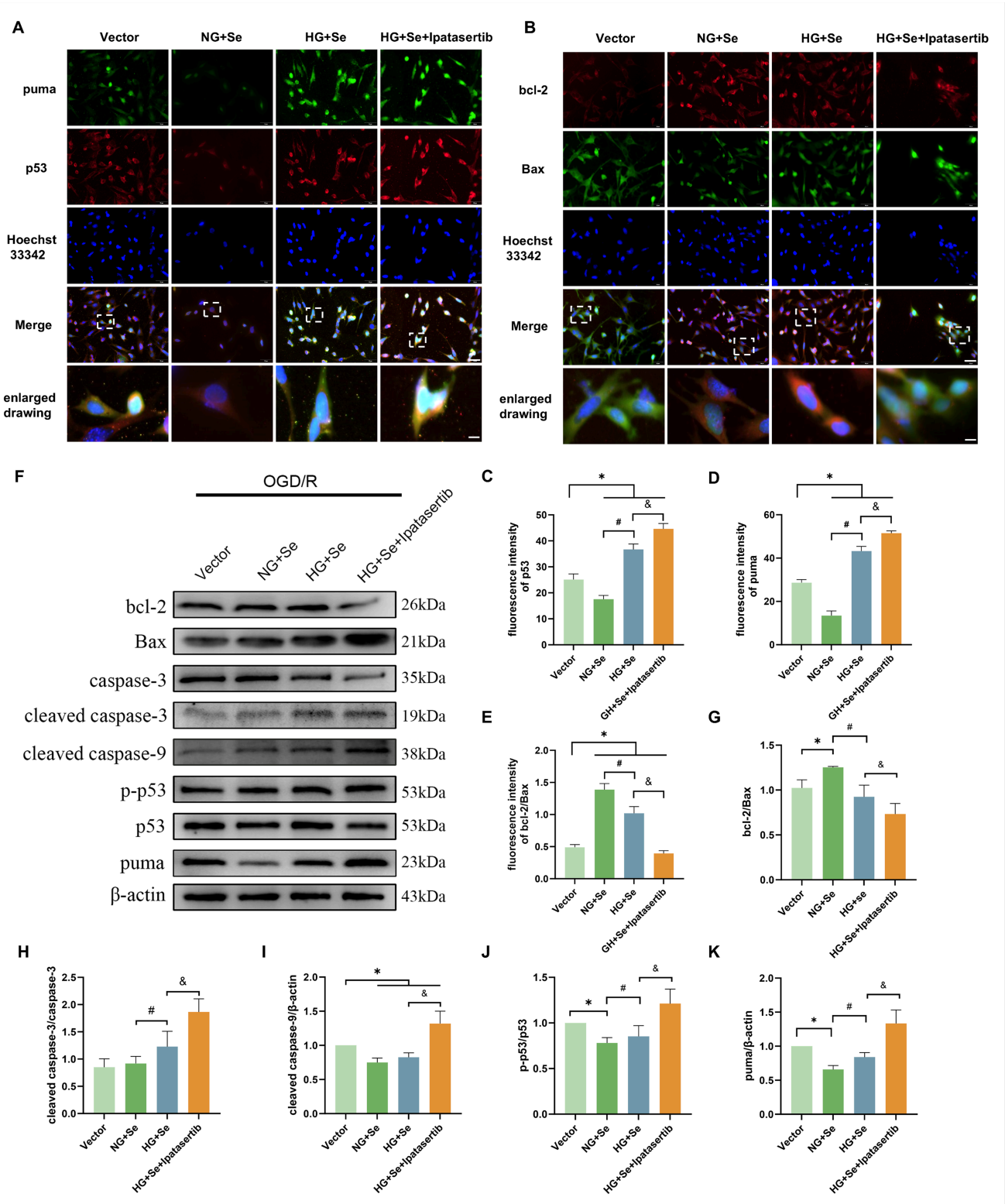


Figure 7

PUMA downregulation reduces cell apoptosis via the p53/PUMA and Bcl-2/Bax signaling pathways. (A) Immunofluorescence co-staining of p53 and PUMA (scale bar = 50 μm, scale bar = 10 μm). (B) Immunofluorescence co-staining of Bcl-2 and Bax (scale bar = 50 μm, scale bar = 10 μm). (C–E) Quantitative analysis of fluorescence intensity. (F) Western blot bands of apoptotic-related proteins. (G–K) Quantitative analysis of apoptotic protein expression levels. *P < 0.05 vs. Vector group; #P < 0.05 vs. NG+Se+OGD/R group; &P < 0.05 vs. HG+Se+OGD/R group

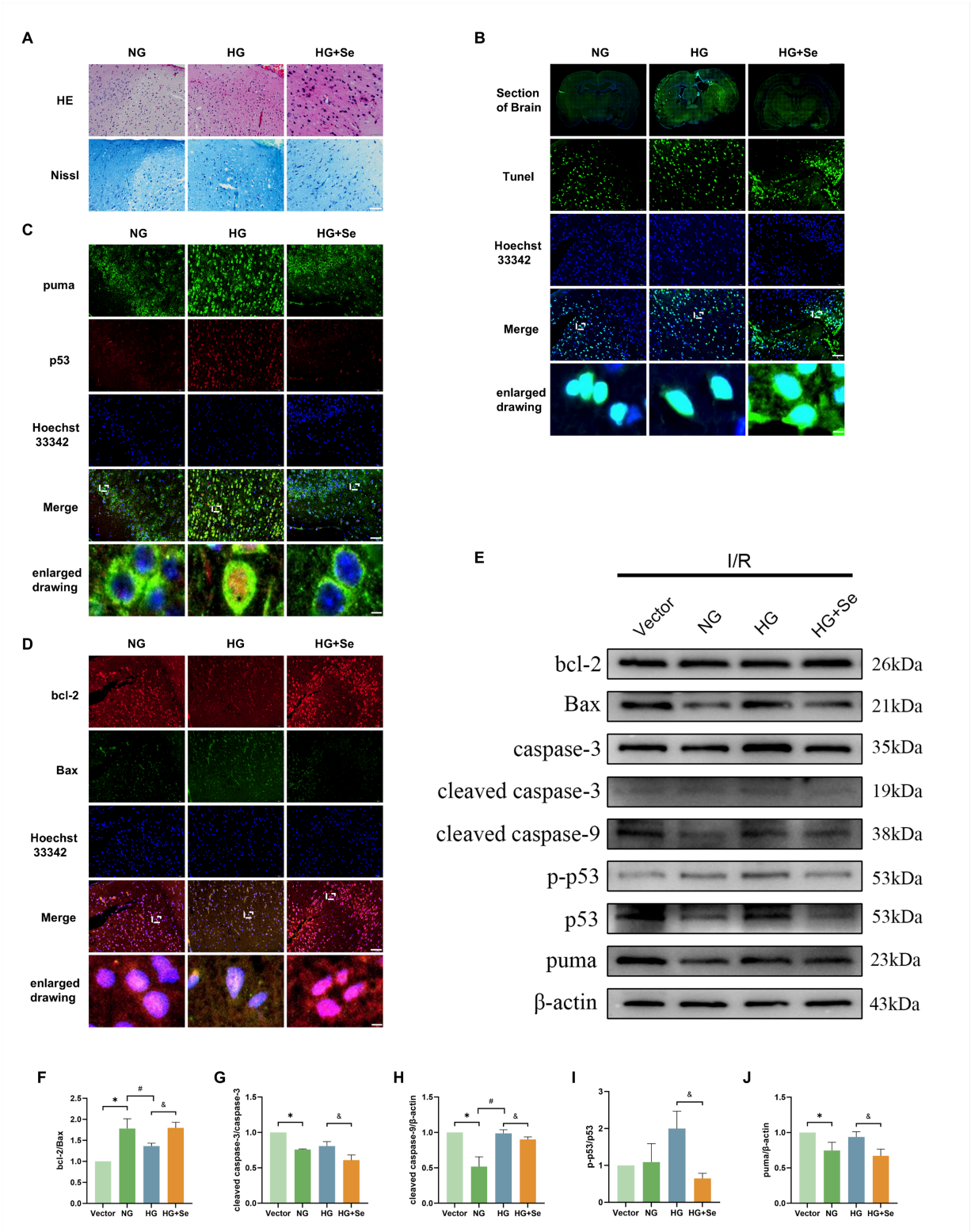


Figure 8

PUMA knockout synergizes with sodium selenite to alleviate hyperglycemia-exacerbated cerebral I/R injury in vivo. (A) HE staining and Nissl staining (scale bar = 50 μm). (B) Representative images of TUNEL staining (scale bar = 50 μm). (C) Immunofluorescence co-staining of p53 and PUMA (scale bar = 50 μm, scale bar = 10 μm). (D) Immunofluorescence co-staining of Bcl-2 and Bax (scale bar = 50 μm, scale bar = 10 μm). (E) Western blot bands of apoptotic-related proteins. (F–J) Quantitative analysis of apoptotic protein expression levels. *P < 0.05 vs. Vector group; #P < 0.05 vs. NG+Se+I/R group; &P < 0.05 vs. HG+Se+I/R group

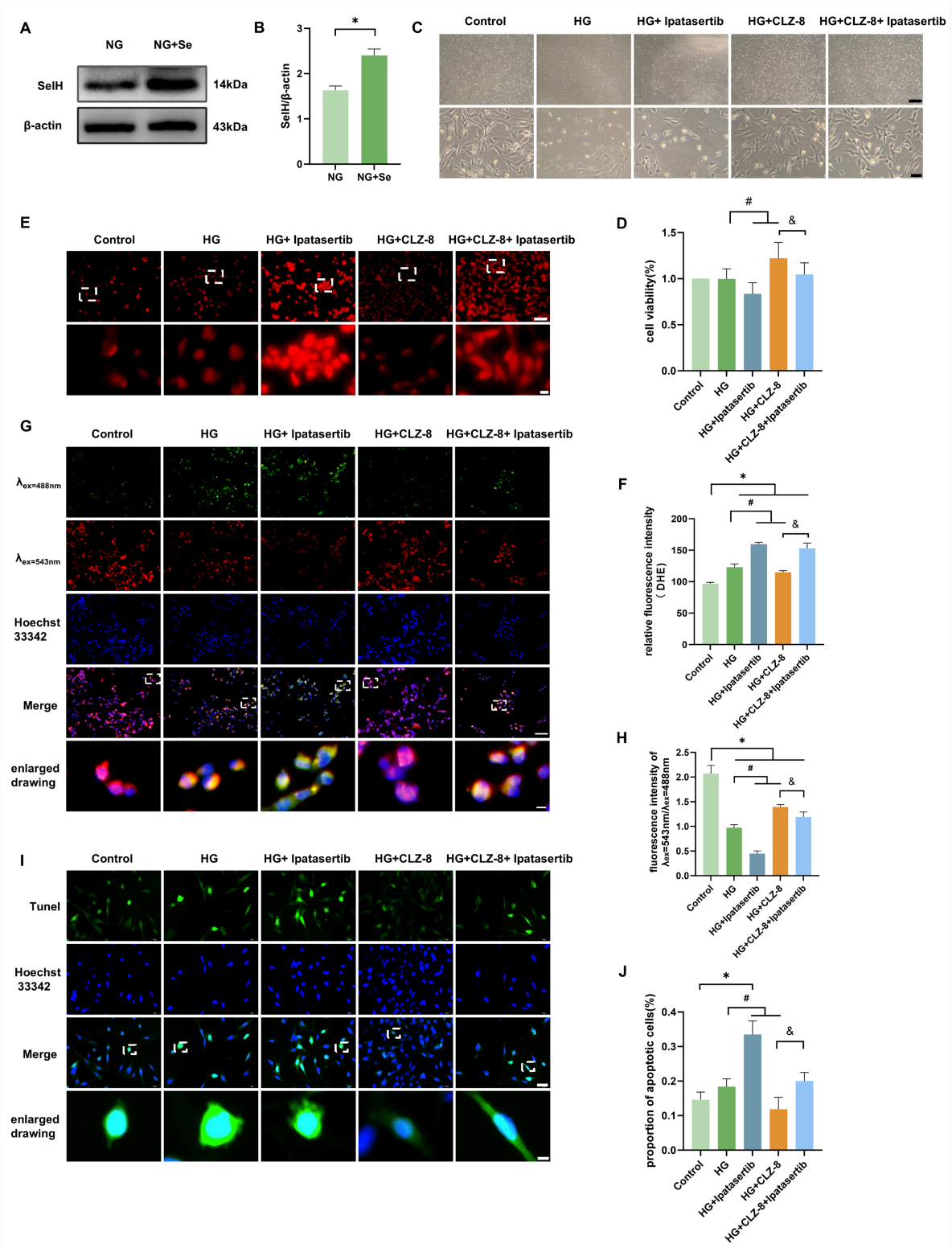


Figure 9

SelH overexpression mitigates high glucose-OGD/R-induced cellular injury by regulating PUMA expression. (A) Western blot bands of SelH protein. (B) Quantitative analysis of SelH overexpression efficiency. (C) Representative images of cellular morphology (scale bar = 50 μm). (D) Cell viability detected by CCK-8 assay. (E) Representative images of ROS staining (scale bar = 50 μm). (F) Relative fluorescence intensity of ROS. (G) Representative images of JC-1 staining (scale bar = 50 μm). (H)

Mitochondrial membrane potential (JC-1) ratio. (I) Representative images of TUNEL staining (scale bar = 50 μm). (J) Quantitative analysis of apoptotic rate. *P< 0.05 vs. Control group; #P < 0.05 vs. HG+OGD/R group; &P < 0.05 vs. HG+CLZ-8+OGD/R group

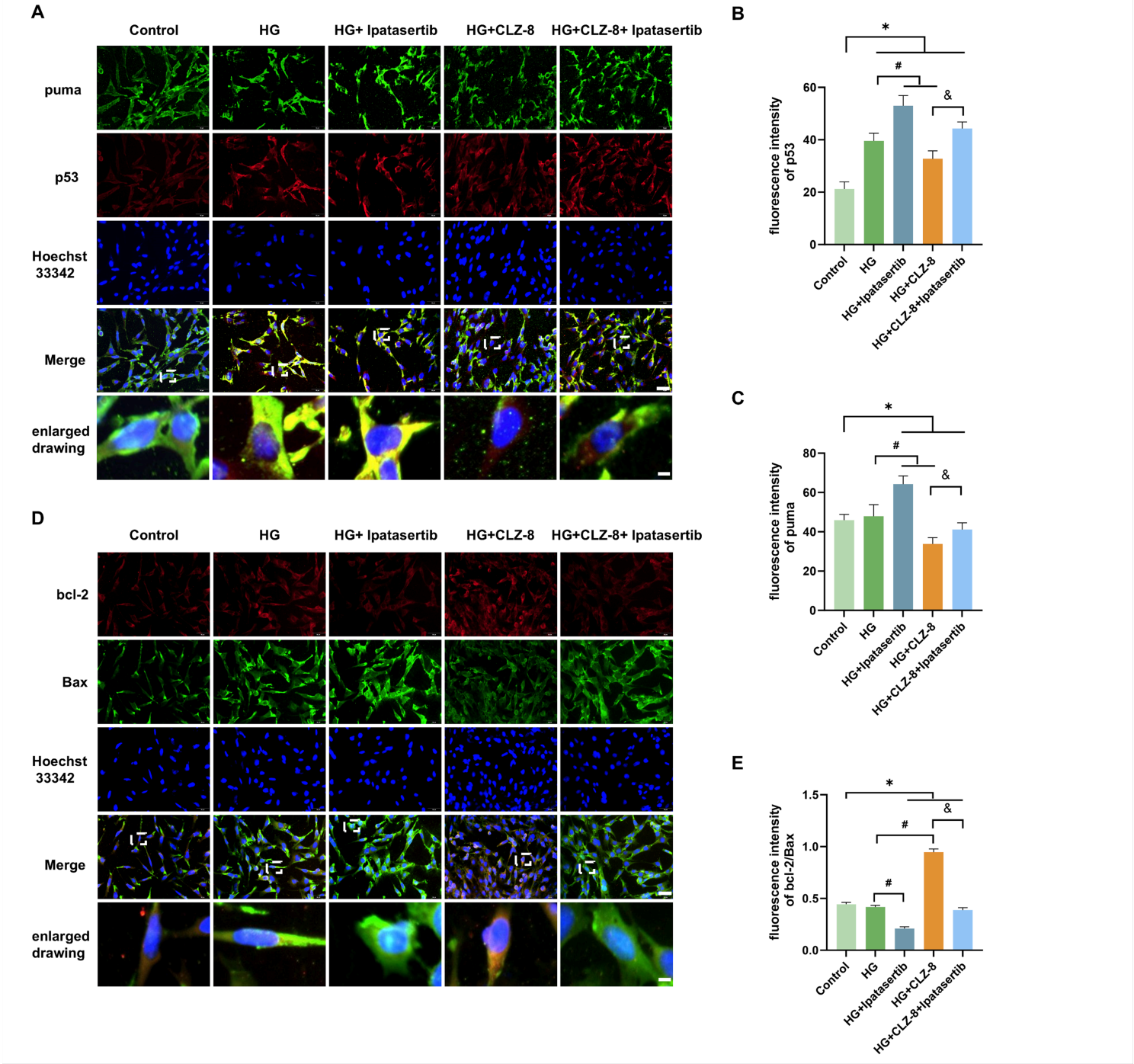


Figure 10

SelH overexpression inhibits cell apoptosis through the p53/PUMA and Bcl-2/Bax signaling axes. (A) Immunofluorescence co-staining of p53 and PUMA (scale bar = 50 μm, scale bar = 10 μm). (B–C) Quantitative analysis of p53 and PUMA fluorescence intensity. (D) Immunofluorescence co-staining of Bcl-2 and Bax (scale bar = 50 μm, scale bar = 10 μm). (E) Quantitative analysis of Bcl-2/Bax fluorescence

intensity ratio. *P < 0.05 vs. Control group; #P < 0.05 vs. HG+OGD/R group; &*P < 0.05* vs. HG+CLZ-8+OGD/R group

Supplementary Files

This is a list of supplementary files associated with this preprint. Click to download.

- WesternBlotsimages.zip